University of New Orleans
ScholarWorks@UNO

University of New Orleans Theses and Dissertations | Dissertations and Theses

5-21-2004

Investigation of Microcrack Growth in [0/90]s Graphite Epoxy Composite Laminates Using X-Ray Microtomography

Arun Tatiparthi
University of New Orleans

Follow this and additional works at: https://scholarworks.uno.edu/td

Recommended Citation

Tatiparthi, Arun, "Investigation of Microcrack Growth in [0/90]s Graphite Epoxy Composite Laminates Using X-Ray Microtomography" (2004). *University of New Orleans Theses and Dissertations*. 95.
https://scholarworks.uno.edu/td/95

This Thesis is protected by copyright and/or related rights. It has been brought to you by ScholarWorks@UNO with permission from the rights-holder(s). You are free to use this Thesis in any way that is permitted by the copyright and related rights legislation that applies to your use. For other uses you need to obtain permission from the rights-holder(s) directly, unless additional rights are indicated by a Creative Commons license in the record and/or on the work itself.

This Thesis has been accepted for inclusion in University of New Orleans Theses and Dissertations by an authorized administrator of ScholarWorks@UNO. For more information, please contact scholarworks@uno.edu.

INVESTIGATION OF MICROCRACK GROWTH IN $[0/90]_S$ GRAPHITE EPOXY COMPOSITE LAMINATES USING X-RAY MICROTOMOGRAPHY

A Thesis

Submitted to the Graduate Faculty of the
University of New Orleans
in partial fulfillment of the
requirements for the degree of

Master of Science
in
The Department of Mechanical Engineering

by

Arun Kumar Tatiparthi

B. Tech, Nagarjuna University, 2000

May 2004

Acknowledgements

I am so thankful for the support I have had from my professors, family and friends. No Herculean task consummated without the support and contribution from a number of individuals. These few paragraphs are an effort to optimize my gratitude towards all those who helped me through out this experience and successful completion of the project. I could not have made it this far without them.

Firstly, I would like to thank **Dr. Paul J. Schilling** who has been my advisor through out my graduate career. His patience, understanding, guidance and encouragement have made my graduate experience an enjoyable one. He has provided me with all sorts of assistance and encouragement, showing his dedication to my academic and professional growth. He is one of the most motivating individuals and amicable persons I have ever come across.

Secondly, I would like to thank **Dr. Melody A. Verges** for taking her time in helping me out with testing the samples and providing valuable information about composites. I also thank her for serving on my graduate committee.

I am grateful to **Dr. Paul D. Herrington** and **Dr. David Hui,** who graciously made time to serve on my graduate committee. Their suggestions on my proposal and dissertation have been very helpful and appreciated.

I really appreciate all my colleagues and friends, Mr. Dileep K Simhadri, Mr. Bhanu P Karedla, Mr. Venkat K Gade and Mr. Kishore Rayasam, for helping me out in the lab and their cooperation throughout the research.

My special gratitude to my mother, sisters and Ms. Seema Sharma for being my motivation with their understanding, support and encouragement.

I would like to thank the Lockheed Martin Corporation, and the National Aeronautics and Space Administration George C. Marshall Space Flight Center for their support in carrying out this work by a Research Grant through Grant/Cooperative Agreement Number NCC8-223 for the National Center for Advanced Manufacturing - Louisiana Partnership.

Dedication

This work is dedicated to my mother, Venkata Lakshmi Tatiparthi, for being so encouraging and her inspiration made me to become an engineer for which I am indebted to her forever. Her keen interest for education has instigated me to pursue higher studies and flourish in my career.

Table of Contents

List of Figures

List of Tables

Abstract

Graphite epoxy composites are being used in aerospace industry and spacecraft applications for their light weight and high strength. As a matter of fact these materials also have some disadvantages like damage which is hazardous when used in cryogenic application. Composite materials IM7/977-2, IM7/5555 and IM7/5276-1 are of interest for the aerospace industry and this research concentrates on study of microcracking, delamination and other defects in the [0/90]s composite laminates of the above materials. These materials were uni-axially tested to pre-determined stress levels and the damages in the material were recorded in the form of microcrack density at different stress levels. In this research work the use of X-Ray Microtomography has proven to be an excellent tool to characterize the crack connectivity and damage information three dimensionally. Dye penetrant technique was also used in this work to enhance the visibility of the cracks.

1. Introduction

1.1 Background and Motivation

In today's fast paced technology and communications era where we look forward to explore many hidden and unexplored territories in the outer space, one main problem is a need for cheaper access to space. To overcome this problem National Aeronautics and Space Administration (NASA) has put forward an initiative to use Reusable Launch Vehicles (RLV) in which the total payload of the vehicle is reduced by fabricating it mostly by using composite materials. Composite materials offer an advantage over the traditional metals used in aircraft manufacturing, as they are light in weight and hence contribute to reduction in the overall payload.

The word composite refers to the combination of two or more materials to obtain a unique combination of properties in the resulting material. These have high strength and stiffness to weight ratio and hence are used widely in aerospace and other critical applications. Composites exclude metal alloys, plastic co-polymers, minerals and wood.

Liquid hydrogen (LH_2) tanks are the largest structural components of RLV's. The design of lightweight fuel tanks is therefore important for reducing the cost of space access. Polymer Matrix Composite (PMC) hydrogen tanks have been proposed by Dixon [Ref 1]

to reduce the weight of reusable launch vehicles. The fuel tanks of these vehicles would be manufactured mainly out of carbon/epoxy to reduce the weight. A study estimated that replacing a conventional fuel tank structure with an all composite one would reduce its weight by 40% and the overall weight of the vehicle by 14% [Ref 2]. The purpose of these tanks is to hold liquid hydrogen at cryogenic temperatures around -423°F. Hydrogen is difficult to store because of its small molecular size and this makes it more prone to leakage. Many factors contribute to the leakage of the gases through the tank, like porosity, manufacturing flaws, and internal damage. Mostly in PMC materials leakage is believed to be because of microcracks which form leakage paths that allow the gases and liquid to pass through the material. It was also noted that the microcracks mostly occur in polymer matrix materials at -473°F (LH_2) temperature because of large thermal residual stresses, large mechanical stresses and low transverse matrix strength [Ref 3]. Generally when the reusable launch vehicle is re-entering the atmosphere at high speeds of around mach 15 with empty fuel tanks, these fuel tanks quickly reach around 260°F and this large variation in temperatures may result in crack initiation through the tanks. Since composites are composed of different ply layers oriented in different directions, a change in temperature will cause the layers to expand in different directions depending on the thermal expansion coefficients of both the fibers and the matrix material. This develops a high amount of strain energy that can be relieved with the formation of cracks. If there exists any kind of inter-connectivity between the cracks in adjacent layers they tend to form a path for the fuel to leak and make the composite structure permeable.

1.2 Project Objectives

Damage in polymer matrix composites occur at much lower loads than the failure load, hence when used in the fuel tank applications the damage in the composite can cause a path for leakage of the fuel that can be catastrophic. Hence there is a need to assess damage in composite materials prior to failure in terms of matrix microcracking, delamination and damage connectivity. This information would give a better picture to understand the induced damage at a particular loading which could cause a leakage condition.

The objective of the present thesis is to study the microcracking behavior in composite materials IM7/977-2, IM7/5555, and IM7/5276-1 under uniaxial tensile loading. The study includes the crack density determination and the types of damages the composite material incurs at different stress levels for different samples. In this study the use of X-ray tomography and optical microscopy have provided useful information regarding the type of damage in the composite laminate, particularly, microcracking which can cause permeability in the cryogenic fuel tank. The main advantage of using the X-ray tomography technique is that it gives three-dimensional information about the damage in the composite non-destructively.

The experimental work consists of five parts: 1) preparation of the samples, 2) tensile loading of the samples to different stress levels, 3) dye penetration into the sample to make the cracks and damage show prominently, 4) investigation for edge cracks in the

samples using optical microscopy and 5) investigation of microcracks and crack connectivity using radiographs from the X-ray microtomography.

1.3 Thesis Outline

This thesis is divided into 6 chapters

- Chapter 1 includes an introduction to the composites and their application, the motivation and background, project objectives and thesis outline.
- Chapter 2 includes a literature review related to composites, the damage they incur during the manufacturing and in service, and the Non-destructive techniques (NDT) methods used to detect these damages.
- Chapter 3 includes a detailed description of the X-ray tomography method which was used to observe the damage in the composite material.
- Chapter 4 includes the step by step explanation of the experimental procedure followed.
- Chapter 5 includes the results and discussion after the experimental work and
- Chapter 6 includes the conclusions drawn from the experimental results.

2. Literature Review

The purpose of this literature review is to provide background information on the issues to be considered in this thesis and to emphasize the relevance of this present study. The topics covered in this chapter are 1) composites and their constituents 2) damage incurred in composites during the manufacturing processes or during service 3) matrix microcracking and delamination 4) and X-ray tomography.

2.1 Composites and their constituents

Composites, as described earlier, are made up of two or more different materials to form a completely different material with unique properties. These mainly consist of a matrix material and a reinforcing material. Reinforcements can be fibers, fabrics, particulates or whiskers and the matrix materials can be metals, plastics or ceramics. Reinforcing materials provide strength and stiffness to the composite, whereas the matrix material binds the reinforcements tightly together to provide rigidity, shape and environmental resistance. A fiber-reinforced composite is made up of different unidirectional plies to provide required stiffness and strength in the specified direction. Each ply is called a lamina and when a number of these plies are stacked up in different orientations (a process called lamination) it is called a laminate. This is shown in the Fig 2.1.

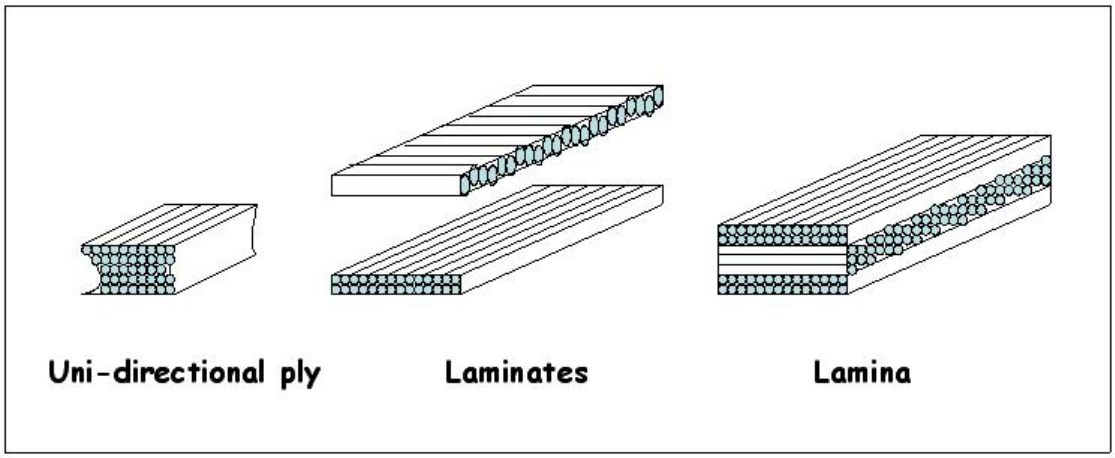

Figure 2.1 *Components of a composite material*

Generally in composites the reinforcements carry 70 to 90% of the load, and provide stiffness, strength, thermal resistance and other properties. The matrix material transfers the load to the reinforcements, provides protection to the reinforcements against chemical and mechanical damage and gives the final desired shape to the composite. Generally reinforcement fibers are subjected to damage during handling and processing due to rupture against each other and the equipment. Hence the fibers are covered with a protective substance called as sizing. Sizing acts as a lubricant and helps a bundle of fibers to stick together and also helps in bonding with the matrix material. Generally sizing is preferred for glass fibers rather than carbon fibers.

2.1.1 Fiber materials

Glass fibers: These fibers have typical properties of hardness, corrosion resistance and inertness. Based on these properties glass fibers are classified into different groups.

E-glass fibers – E for Electrical, used for electrical and chemical resistant applications.

S-glass fibers – S for Strength, used for high strength applications.

C-glass fibers – C for Corrosion, used for corrosion resistance applications.

D-glass fibers – D for Dielectric, used for electrical applications as core reinforcement.

A-glass fibers - A for Alkaline, used for alkaline resistance applications.

Carbon/Graphite fibers: These fibers are light in weight and have excellent strength properties. The properties of these fibers depend on the raw materials used to manufacture them, like either Polyacrylonitrile (PAN) or Pitch. Pitch fibers have low strength than PAN. Some of these fibers are

AS & HS – High stiffness fibers

IM – Intermediate modulus fibers

HM – High modulus fibers

UHM – Ultra high modulus fibers

P100/400 – Pitch based fibers

Organic fibers and other fibers: Popularly know organic fibers are aramid fibers under the trade name Kevlar, Technora, Twaron. These fibers absorb moisture, creep and are sensitive to UV rays. Other known fibers are boron fibers, silicon carbide fibers and ceramic fibers.

2.1.2 Matrix materials

Thermoset matrices: Thermosets are formed by an irreversible chemical reaction called curing, in which they form 3D molecular cross-links in the form of chains which prohibit them from reforming and remolding once cured. These thermosets shrink once they are

cured and hence induce internal stresses, cracking, fiber misalignment and dimensional inaccuracy to the composite. These thermoset materials are prone to corrosion and are recommended for refrigerated storage. These are easy to process as they have low viscosity.

Thermoplastic matrices: Thermoplastics are softened from solid state to be processed and they have high viscosity and need high temperatures for softening which makes them difficult for processing. These do not undergo any curing process and hence these can be repaired by reforming and remolding. Thermoplastics are not affected by corrosion and hence they have unlimited shelf life.

The main concern of this thesis is on carbon–epoxy composites and their damage during tensile testing. Here carbon fibers act as the reinforcing material and epoxy as the matrix material. Carbon fibers have excellent chemical resistance and high strength along the axial direction. Carbon–epoxy composites can be manufactured using any of the available processes in the market like hand lay-up, vacuum bagging, autoclave processing, compression molding, resin transfer molding (RTM), and pultrusion.

The samples which are used in this research were cut from panels of carbon-epoxy composite manufactured by hand lay-up and vacuum bagging at the Lockheed Martin Michoud facility. Different types of damage occur in composites which might be due to the manufacturing process or due to the load application in service.

2.2 Types of Damages in Composites

It is well known that the defects and damages in laminated composites reduce the strength, stiffness and also the safe working life of the composite structures. Defects may be introduced during manufacture, accidentally in-service or perhaps unavoidably in design because of the requirement to introduce discontinuities such as cutouts, ply drops or structural connections [Ref 4, 5].

The defects commonly introduced to composite materials during manufacturing and processing are inclusions, de-bonding, fiber misalignment, voids and residual stresses.

Inclusions – Accidentally included materials during manufacturing like peel paper can have degrading effect on the mechanical properties.

De-bonds –The failure of the interface between the fibers and the matrix material which leads to separation between them, called De-bonding. De-bonding can occur because of poor consolidation or as a result of an inclusion.

Fiber misalignment – This is damage especially prevalent in low fiber volume fraction materials.

Voids – Voids are due to inclusion of air, solvents or other contamination during mixing of resin.

Residual stresses – These stresses are mainly caused by the curing process. These affect the mechanical properties and can cause warping, fiber buckling, micro-cracking of the matrix and delamination. The cause of these stresses is mainly the difference in thermal expansion of the fiber and matrix material in different directions.

The defects commonly introduced in composite materials during the service like loading are matrix cracking, fiber breakage, fiber pull-out, delamination, and fiber-matrix debonding. Figure 2.2 shows a composite panel, with 0deg plies on the outside and the 90deg plies in the inside, uniaxially loaded to a stress of σ_x. The damages incurred in the composite laminate due to this uniaxial tensile loading are discussed below.

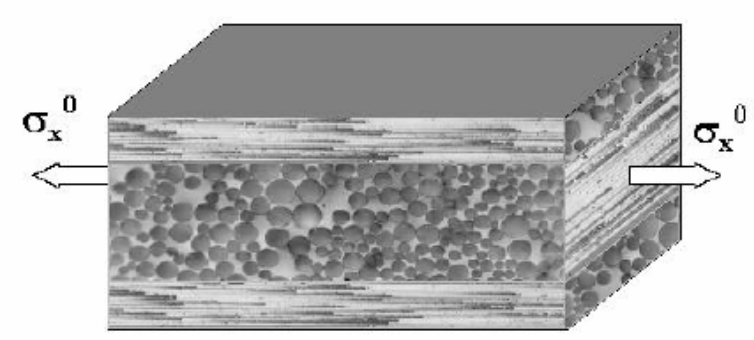

Figure 2.2 *Cross-ply laminate subjected to uniaxial loading [Ref 6]*

Fiber-matrix debonding: This is the first mode of failure that occurs in the composite material uniaxially loaded because of the poor interface bonding between the fibers and the matrix. These debondings link together to form large scale damage called Matrix cracking. Figure 2.3 shows the matrix crack formed due to fiber-matrix debonding.

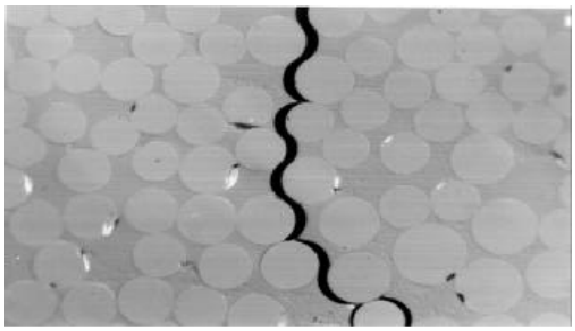

Figiure 2.3 *Propagation of a matrix cracking due to Fiber-matrix debonding [Ref 6]*

Matrix cracking: As described by R.Joffe [Ref 6], the cracks are initiated from the interface failures. Multiple debonding between the fibers and matrix occurs and these debonds are connected and transverse cracks or matrix cracks are formed. These microcracks are catastrophic because they reduce the load carrying capacity of the structure in the direction normal to the cracks and reduce the stiffness in that direction. A more detailed explanation about these microcracks is given in Section 2.3. Figure 2.4 shows matrix cracking of a cross-ply laminate subjected to uniaxial tension.

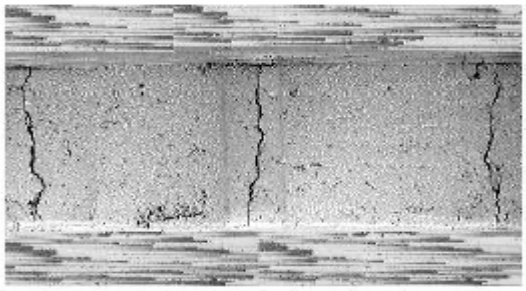

Figure 2.4 *Matrix cracking in a cross-ply laminate [Ref 6]*

Delamination: Delamination is a form of failure that occurs on a plane between adjacent layers within a laminate. Microcracks introduce multiple stress concentration points at the crack tips as the microcracks are restrained by the adjacent layers. These crack tips exist at the interface between piles of a laminated composite and thus lead to delamination which is a large scale damage. Delamination can increase connectivity of the matrix cracks and cause leakage paths to fuel when the structure is used as a pressure.

Fiber breaking: When composites are subjected to tensile loading because of poor interfacial bonding microcracks are formed. These microcracks lead to delamination and fiber breaking would be the next mode of failure after delamination. Since the adjacent

layers with no microcracks tend to bear the entire applied load, their fibers tend to crack leading to fiber breakage.

Fiber pull-out: This damage, Fiber pull-out, occurs prior to fiber breakage. The fibers get pulled out of the matrix on tensile loading. Figure 2.5 shows both the fiber breakage and fiber pull-out.

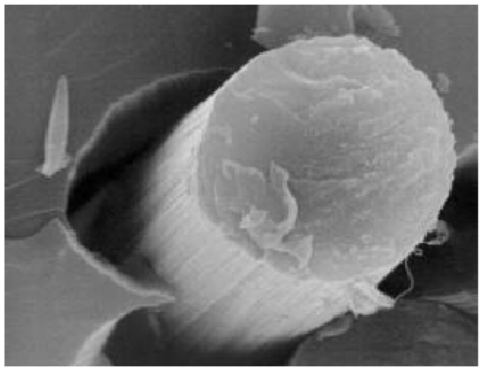

Figure 2.5 *Fiber breakage and fiber pull-out due to poor bonding Between fiber and matrix interface [Ref 6]*

Fracture: This is the final stage of failure where the material breaks and separates out. This fracture might be in the form of complete detachment of the materials or constrained ply cracking.

Figure 2.6 shows the various damages observed in composite material when subjected to uni-axial stress. The modes of damage shown in Figure 2.6 are based on the information collected from different researchers and their publications.

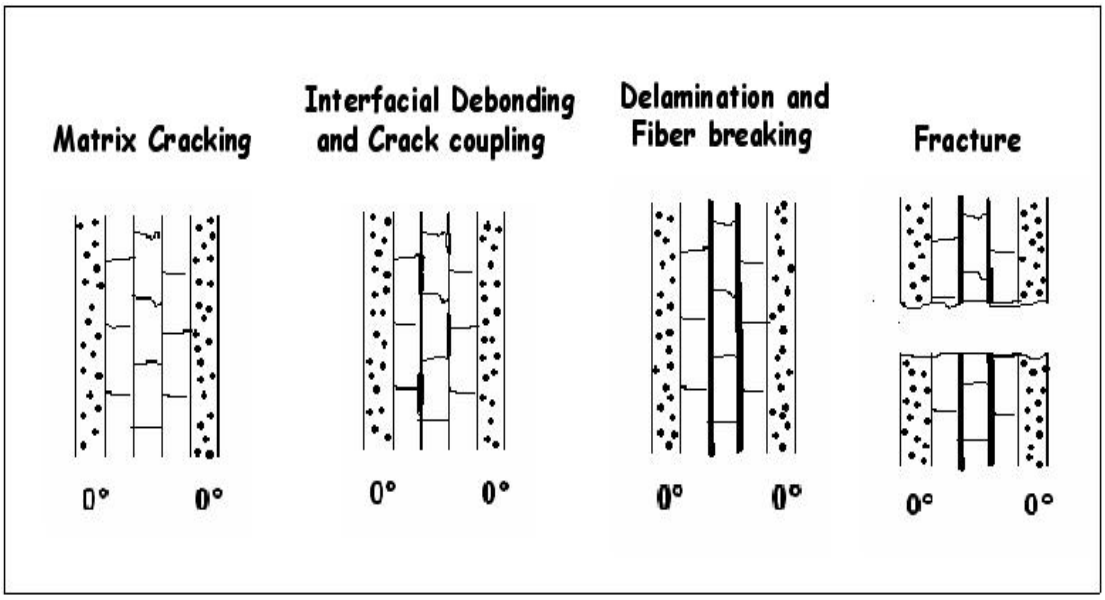

Figure 2.6 *Modes of damage in a composite material [Ref 7]*

2.3 Matrix Microcracking

As described by Nairn et al. [Ref 8] the first form of damage in composite laminates is usually matrix microcracking. Matrix microcracking is one of the most common forms of damage encountered in composite materials and is often a precursor to overall failure. Microcracking is the cracking of the matrix material due to transverse loading in the cross-ply laminates. These microcracks run all the way through the thickness of the ply and parallel to the fibers in the ply. These are usually transverse to the main loading direction and thus also called transverse cracks. According to R. Joffe [Ref 6], these microcracks are initiated from the interface failures, as a result of it multiple debonding between the fibers and matrix occurs and these debonds are connected and transverse cracks or matrix cracks are formed. Other studies [Ref 9, 10] have observed that microcracks in the 90º ply of a $[0/90]_s$ cross-ply laminate occur at laminate tensile strains as low as 0.2 to 0.3%.

Matrix microcracking can develop under tensile loading, fatigue loading, thermal loading or impact conditions and hence are more commonly due to in-service effects. Microcracks due to thermal loading or thermal residual stresses are formed due of the difference in the thermal expansion coefficient between the fibers and the matrix material. Generally the matrix material has greater thermal expansion coefficient compared to the fibers and hence, when a thermal load is applied to the composite due to this difference in thermal expansion coefficient the matrix material tries to expand more than the fibers and this leads to debonding of matrix with the fibers at the weakest matrix-fiber interface region. Further application of this thermal load leads to large scale damage, called matrix microcracking.

Microcracking degrades the thermomechanical properties of the laminate like poison's ratio and thermal expansion coefficient and hence often leads to overall failure. The first microcrack causes very little degradation in the thermomechancial properties of the composite laminate but upon continued loading the laminate tends to crack more forming multiple microcracks. This multiple microcracking causes more degradation in the thermomechancial properties of the laminate. The growth of multiple microcracking was explained by Groves et al [Ref 11]. At low crack density, both the maximum axial stress and the maximum principle stress in the 90º plies occur midway between the existing microcracks. Thus at low crack density the new cracks try to form midway between the existing cracks and develop into periodic array of cracks as shown in Figure 2.7.

In most cases growth of microcracking from a practical point of view is instantaneous across the thickness of the affected ply (or plies). At high crack density, i.e. higher number of cracks per unit length, the microcracking shows a slowing down trend and gradually reaches saturation in the damage state which is called "Crack Density Saturation" (CDS) in the microcrack density vs. stress plot. At high crack density, interactions between the microcracks cause the maximum principle stress to shift near the 0/90 interface and close to an existing microcrack [Ref 11, 12]. The adjacent layers, which will typically have fibres at a different orientation to that in the affected layer, usually act as crack stoppers. Hence these layers often restrain any further through thickness growth. Figure 2.7 shows the schematic of microcrack development in the 90º plies of a typical composite material at different stress levels.

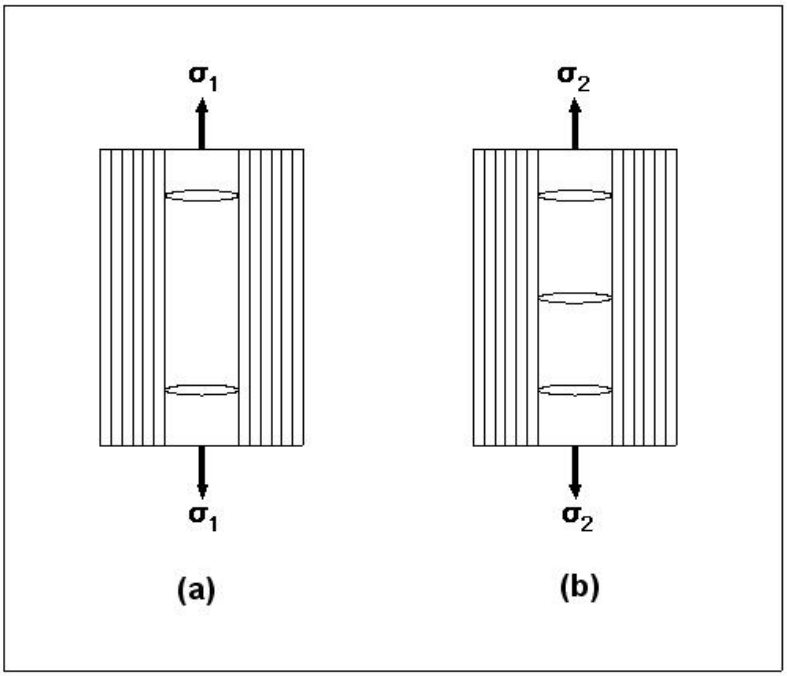

Figure 2.7 *Schematic of microcrack development in the 90° ply at different stress levels. (a) Microcrack development at an applied load σ_1. (b) Formation of microcrack in the middle of existing cracks at applied load σ_2 ($\sigma_2 > \sigma_1$).*

Many experiments have been done by Garrett and Bailey [Ref 13-15] on glass reinforced polyester $[0/90]_s$ and glass reinforced epoxy $[0/90]_s$ laminates to calculate the strain required to initiate microcracking in composite materials. They continuously varied the thickness of the 90º plies keeping the thickness of the supporting 0º plies constant. Their results indicate that on decreasing the thickness of the 90º plies less than that of the 0º plies, the strain to initiate microcracking in the 90º plies increases and a vice versa effect is also true in this case, i.e. increasing the thickness of the 90º plies would make the cracks to form almost instantaneous as the strain to initiate microcracking decreases. At a certain decrease in thickness of the 90º plies the cracks were partially and totally suppressed. Similar experiments were conducted on the carbon-epoxy laminates by Bailey, Curtis and Parvizi [Ref 16, 17] and found that the strain to initiate microcracking increases as the thickness of the 90º plies decreases.

Flaggs and Kural [Ref 18] also tested many carbon-epoxy laminates with different ply orientations. They found that the in-situ failure strain is always greater than the transverse failure strain. In the experiments conducted above [Ref 16-18], the microcracks in the carbon-epoxy laminates always formed instantaneously across the entire cross sectional area of the 90º plies. The thinnest of the 90º plies tested was half the thickness of the 0º plies and they could see no partial or total suppression of the microcracks [Ref 18].

Experiments conducted on the $[90_n/0_m]_s$ laminates [Ref 19-25] with the 90º plies on the outside show that the strain to initiate microcracking in the $[90_n/0_m]_s$ laminates with the 90º plies on the outside is lower when compared to the $[0_m/90_n]_s$ laminates with 90º plies

in the middle. This result can be supported as the surface 90º plies in the $[90_n/0_m]_s$ laminates are constrained only on one side by the adjacent 0º plies where as in the $[0_m/90_n]_s$ laminates the 90º plies are constrained on both sides. A study [Ref 23-25] on $[90_n/0_m]_s$ and $[0_m/90_n]_s$ laminates shows that the microcracks start sooner in $[90_n/0_m]_s$ laminates but the $[0_m/90_n]_s$ laminates eventually develop more microcracks at saturation. Figure 2.8 shows the schematic of the microcrack behavior in the $[0_m/90_n]_s$ and $[90_n/0_m]_s$ laminates.

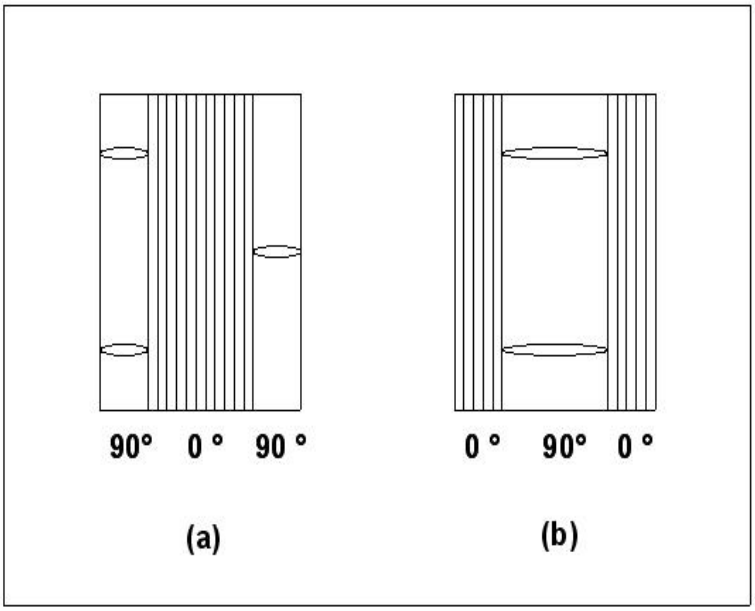

Figure 2.8 *Schematic of microcrack behavior in*
(a) [90n/0m]s laminate and (b) [0m/90n]s laminate

Lavoie and Adolfsson [Ref 26] found that when $[+\theta_n/-\theta_n/90_{2n}]_s$ class of laminates subjected to fatigue or monotonic loading shows a high density form of matrix cracking called stitch cracking. They also found that this form of stitch cracking is not only due to fatigue or monotonic loading but can form even due to thermal residual stresses. Their

results indicate that the stitch cracks form in the constraint plies oriented at some angle θ upon microcracking in a 90º ply, when the included angle between the constraint ply and the 90º ply was less than 50º. When long microcracking was observed in the +θº plies then stitch cracks formed in certain -θº plies.

Microcracking also nucleates other forms of damage like delamination, fiber breakage, fiber pull-out and fracture. In cryogenic fuel tank applications, such damage causes leakage of the fuel and often becomes hazardous. The main concern of this research work is to detect the internal damage in composite materials like microcrack, delamination and inter connectivity of the microcracks which forms a path for the fuel to seep out if used in cryogenic fuel tank applications. As described by Nairn [Ref 27], a logical experiment to characterize the microcracking properties of composite laminates is to follow the microcracking process and record the number of microcracks or microcracking density as a function of applied load. These experiments were carried out by many researchers on a number of different lay-ups and found some interesting information from them. This present research work consists of determining the microcrack density at different stress levels and finding the type of damage at each level of the stress using X-ray microtomography.

2.4 Delamination

Delamination is a form of failure which occurs on a plane between adjacent layers within a laminate. Once the delaminations begin, they propagate on continued loading while additional microcracking slows down or stops [Ref 30]. This failure might be because of inadequate adhesion between the layers or due to microcracking and other reasons which are summarized below. In the discussions below the specimens are tested under uniaxial tension.

Matrix-microcracking in the through thickness direction within individual layers of a laminate can give rise to delaminations [Ref 28]. Microcracking generally appears perpendicular to the fiber direction within a layer and extends through the entire thickness of that layer. Since the microcrack extends through the entire thickness of the affected layer, there is a possible chance for it to open at the middle region of the affected layer as the crack tips are restrained by their respective adjacent layers. Due to this restraint, a multi-axial stress state is developed at the crack tip with strong through thickness tensile components. These tensile stresses may be sufficient to initiate interlaminar failure from the crack tips [Ref 29, 30]. Hence as the microcrack density increases delamination are also increases. Delamination from the tips of the microcracks increases as the thickness of the 90º ply increases with the thickness of the 0º plies being constant [Ref 8, 38].

Impact often causes local delamination in the composite laminate. Even though the impact might be transverse to a laminate, damage will often propagate significantly along

the planes between adjacent layers since these planes are not benefited by the reinforcing effect of fibers and are more susceptible to damage. Hence sites of impact often form zones of interlaminar splitting. Growth of the defect occurs however by extension of the delamination into the surrounding material that might not have been directly affected by the initial impact event.

As described by Stone [Ref 31], through thickness failures arising from overload or fatigue can also develop into delaminations. Laminated composites tend to be weak in the through thickness direction and are also sensitive to loads giving rise to stresses in the through thickness direction. The stresses of concern here are direct through thickness tension and through thickness shear. It is interesting to note that the stresses giving rise to delamination may be small in magnitude (especially by comparison to typical laminate in-plane stress) and often exist as secondary effects [Ref 32]. Through thickness stresses may also be developed at the edges of laminates, even when no externally applied through thickness tension or shear loads exist [Ref 33, 34]. These through thickness stresses are usually smaller than the applied in-plane stresses but since they act in a direction that is relatively weak, static or fatigue failures, giving rise to delaminations can arise.

Another study [Ref 35-37] says that, the presence of multiple matrix cracks in the 90º ply can precipitate matrix cracks in other plies. As the applied strain increases the transverse stress leads to longitudinal splitting of 0º plies [Ref 16, 17]. Longitudinal splitting of the 0º ply forms parallel to the applied tension and crosses over the 90º transverse cracks, so

the interaction between these two crossing cracks gives rise to a highly magnified three-dimensional stress field. The interlaminar tensile and shearing components of this stress field then cause 0/90 interface delamination [Ref 38]. Further loading causes the propagation of many localized delaminations resulting in 0/90 interface separation.

One more factor which causes delamination is the weak bonding between the adjacent layers of a composite laminate. This might be because of improper wet out of the layers or improper removal of backing from the prepreg. This source of delamination would be of concern in the long run of the composite laminate.

2.5 Non-destructive Techniques

Non-destructive testing (NDT) has been practiced for many decades. One of the earliest applications was the detection of surface cracks in railcar wheels and axles. The parts were dipped in oil, then cleaned and dusted with a powder. When a crack was present, the oil would seep from the defect and wet the surface providing visual indicating that the component was flawed.

Non-destructive testing is a very broad field which plays a critical role to assure that structural components and systems are performing their function in a reliable and cost effective manner. NDT allows parts and materials to be inspected and measured without damaging them and allows inspection without interfering with a product's final use; hence NDT provides an excellent balance between quality control and cost-effectiveness. Generally speaking, NDT applies to industrial inspections.

Non-destructive Evaluation (NDE) is a term that is often used interchangeably with NDT. However, technically, NDE is used to describe measurements that are more quantitative in nature. For example, a NDE method would not only locate a defect, but it also used to measure defect's size, shape, and orientation. NDE may be used to determine material properties such as fracture toughness, formability, and other physical characteristics. Researchers however keep finding new and better methods of NDT to detect the defects and make the method more cost effective. Several methods of NDT used in the industry are described below.

2.5.1 Visual and Optical Testing (VT)

Visual inspection involves using the naked eye to look for defects. In this method use of special tools such as magnifying glasses, mirrors, or borescopes help to gain access and more closely inspect the specimen area. Visual examiners follow procedures that range from simple to very complex. This technique is used to find only surface cracks and irregularities. But for composites the main failure criteria which are of interest, microcracking cannot be visualized by this technique.

2.5.2 Ultrasonic Testing

Ultrasonic testing (UT) uses transmission of high-frequency sound waves into a material to detect imperfections or to locate changes in material properties. The most commonly used ultrasonic testing technique is pulse echo, where sound waves, generated by a piezoelectric transducer, are introduced into a test object and reflections (echoes) are returned to a receiver from internal imperfections or from the part's geometrical surfaces.

A number of ultrasonic evaluation methods – such as A, B, and C-scans have been used to study various types of flaws in composite materials. The UT A-scan provides only one-dimensional defect information. The UT A-scan is commonly used to measure material thickness as the A-scan signal displays the pulse and amplitude against time. The UT B-scan displays a parallel set of UT A-scans with two-dimensional data (i.e., the B-scan presents defect distribution through the material's cross section). The B-scan can also be used to inspect rotating tubes and pipes, because it provides a cross-sectional view of defect distribution. The UT C-scan is the most widely used scan mode, as it provides the two-dimensional information of defect distribution. A C-scan displays the size and position of flaws in an area parallel to the surface. Ultrasonic testing is used for inspecting a wide range of materials like thick and thin section welds, composite structures and adhesively bonded structures. The method is particularly sensitive to lamination and linear type defects.

The limitations of Ultrasonic testing when used for composites are

1) The sensitivity of this technique is poor, i.e., the ability of the instrument to detect the small amount of energy reflected from a flaw is very poor and

2) The resolution of this technique is poor, i.e., the ability to detect flaws lying close to the surface or close to one another is very poor.

2.5.3 Acoustic Emission Testing

In Acoustic Emission (AE) an elastic wave, in the range of ultrasound usually between 20 KHz and 1 MHz, is generated by the rapid release of energy from the source within a

material. The elastic wave propagates through the solid to the surface, where it can be recorded by one or more sensors. The sensor is a transducer that converts the mechanical wave into an electrical signal and hence records the existence and location of possible sources. Since AE signals are very weak they are pre-amplified and then filtered to remove noise. These filtered signals are sent to signal conditioner to get the required information. Ultrasonic testing actively probes the structure whereas acoustic emission listens for emissions from active defects and is very sensitive to defect activity. AE analysis is a useful method for the investigation of local damage in materials.

One of the advantages compared to other NDE techniques is the possibility to observe damage processes during the entire load history without any disturbance to the specimen.
The disadvantages of Acoustic Emission when used for composites are
1) This method can only estimate qualitatively how much damage is in the material and for quantitative results we may need to look for some other NDE methods.
2) Service environments are generally very noisy, and the AE signals are usually very weak, thus, signal discrimination and noise reduction are very difficult.

2.5.4 Eddy Current Testing

Eddy current testing is a method based on the principles of electromagnetic induction. This method is used to detect surface and near-surface discontinuities, changes in material properties, measure conductivity, and measure thickness of nonconductive coatings. A change in magnetic field is generated when alternating current is passed through a coil. If this coil is placed near a conductive material (specimen), the magnetic

field will be generated in the specimen too. The magnetic field in turn creates eddy currents, which produce EMFs (electro-motive forces) in the exciting coil(s) or an auxiliary coil. The phase and amplitude of the EMFs reveal characteristics of the specimen, including presence or absence of defects. This method does not require direct contact with the part being inspected, thus it is truly a nondestructive inspection technique.

2.5.5 Radiography

Radiography uses differential absorption of x-rays, gamma rays or neutron radiation penetrating a test specimen. A receiving end records the image in the form of radiographs to detect the features and internal structure of the specimen that exhibit a difference in thickness or physical density as compared to the surrounding material. This image is a result of difference in attenuation rates, or absorption, for various types of matter. Radiographic attenuation might be affected by dissimilarities in material properties, which causes some difficulties in the interpretation of radiographs. The other applications of radiography in non-destructive testing are radioscopy (real time radiography), computerized tomography (CT), microfocus radiography, and flash radiography.

Radioscopy produces the image of the specimen on the screen rather than on the film, so that very little time lag occurs between the specimen being exposed to radiation and the resulting image. In this technique the image is produced on the screen when the radiation passing through the specimen interacts with the fluorescent screen. In this technique the resolution of the images are not as good as those for images produced on film [Ref 39].

Computed Tomography is a very useful technique to get the 2-D and 3-D cross-sectional images from the flat X-ray images by using radiographic penetration capabilities and principles of optics [Ref 39].

Microfocus radiography uses very small source of X-rays, with less than 40micron spot size, to identify the minute defects in the specimens. This technique varies from the conventional radiography by placing the specimen close to the source in order to magnify the image on to the screen, which is placed at a distance farther than in the conventional set-up.

Flash radiography uses radiography with high power and short duration pulses. The radiation source in this technique is created by discharging a series of capacitors into a field emission x-ray tube of low impedance. The duration of the pulse of radiation is approximately 30 nanoseconds long. The images are captured using fluorescent intensifying screens. Contrast and resolution for this technique are not as good as that for conventional radiography because of the limited radiation available and the relatively large focal spot of the sources [Ref 39].

2.5.6 Magnetic Particle Testing

Magnetic particle testing detects surface and near surface defects in ferromagnetic materials only. This method is accomplished by inducing a magnetic field in a ferromagnetic material and then dusting the surface with iron particles (either dry or suspended in liquid). Surface and near-surface imperfections distort the magnetic field

causing a “leakage field” and concentrate iron particles near imperfections, previewing a visual indication of the flaw.

2.5.7 Dye Penetrant Testing

Liquid penetrant testing is a non-destructive method used to detect surface breaking defects in any nonporous material. The surface of the part under evaluation is coated with a penetrant in which a visible or fluorescent dye is dissolved. The penetrant is pulled into surface defects by capillary action. After some time insuring that the dye has penetrated into the narrowest cracks, the excess penetrant is cleaned from the surface of the sample. A white powder, called developer, is then sprayed or dusted over the part. The developer lifts the penetrant out of the defect, and the dye stains the developer. Then by visual inspection under white or ultraviolet light, the visible or fluorescent dye indications are located, thereby defining the defect. One limitation to this technique is that the material must have a relatively smooth, nonporous surface.

2.5.8 NDT of composites

Different non-destructive techniques are in practice both in the industry and research to find the defects and flaws in composite materials. A few of these techniques and their capabilities to detect the damages are summarized below in Table 2.1.

Table 1 Various NDT methods used to detect the defects in composites

DEFECT TYPE	X-RAY TOMOGRAPHY	ULTRASONICS	EDDY CURRENT	ACOUSTIC EMISSION	VISUAL INSPECTION	DYE PENETRATE
Voids/Porosity	Yes	Yes	No	No	No	Only surface porosity
Debonds	Yes	Some	No	Some	No	Only surface debonding
Delamination	Yes	Some	No	Some	Only edge delamination	Only edge delamination
Broken fibers	Yes	Some	Yes	Yes	No	No
Micro cracks	Yes	Yes	Some	Some	No	No
Matrix cracking	Yes	Yes	Yes	Yes	Only surface matrix cracking	Only surface matrix cracking

3. X-Ray Microtomography

X-ray tomography is a non-destructive technique used in industry to get high resolution images of the internal microstructure of the material of interest. This technique is quiet familiar in the medical world by the names of CT, CAT scans, etc., but is less known as an imaging technique for detecting internal flaws and damages in materials.

3.1 Background of Radiography

The need to find out the internal structure of a specimen without physically destroying it arises in many cases and the solution for this problem was given by Wilhelm Rontgen in 1895 by discovering X-rays [Ref 40]. X-rays are high energy electromagnetic radiation produced when highly energetic electrons interact with matter. For use in X-ray imaging, X-rays are generated by bombarding a metal target, usually tungsten, with high-energy electrons. These X-rays pass through the specimen and make it possible to acquire the internal information about the specimen's structure and other details.

Basic radiography consists of an X-ray source or energy source, collimator, specimen stage, and a detector or screen. The radiating source which basically is an X-ray tube releases X-rays when the metal target is excited. An X-ray beam is typically "steered" by a collimator, which simply removes those photons going in undesired directions. A

collimator is not a lens but a block of absorbing material with one or more holes in it called apertures. These X-rays after passing through the collimator penetrate through the specimen and then hit the detector. Numerous technologies exist for X-ray detection [Ref 41, 42]. These detectors will give a signal proportional to the number of photons striking the detector element. This can be a voltage or a simple photon count; hence the detector response is energy-dependent.

The X-ray image is also called as radiograph or radiogram. This image is formed basically by the difference in the absorption rate or attenuation rate of the X-rays by the specimen. X-ray systems do not directly measure density; they measure the absorptivity, also called the linear absorption coefficient. This is dependent on the density and also on the atomic number *Z* of the element. The energy of X-rays can be increased by increasing the voltage which in turn decreases the wavelength but improves the penetration ability [Ref 43] and by increasing the current the numbers of X-rays are increased.

3.2 Computed Tomography

Conventional techniques, such as electron or optical microscopy, can provide only surface information, and must be treated or sectioned if wanted to know the internal structure of the specimen. However, many samples cannot be investigated in this way, as sectioning may be impracticable or can damage the specimen. In such cases imaging techniques are required and computed tomography satisfies this demand. This technique gives us the 2D x-ray images or cross-sectional images called tomograms at different rotation angles of the specimen with a resolution typically to the order of several microns.

The invention of Computed tomography (CT) in the early 1970's by Hounsfield, made it finally possible to reconstruct the three dimensional structure of the specimen with a computer using the X-ray pictures or 2D x-ray images taken at different rotation steps of the specimen. By reconstructing these 2D images we get the 3D image of the specimen with internal microstructural information. By reducing the focal spot size we can go for large magnifications on the specimen and get high spatial resolution. For this very high resolution the above technique is also called as X-Ray MicroTomography. Computed tomography provides an accurate image of variations of X-ray absorption within a specimen, regardless of the phase constituents or varying density gradients of the specimen.

In computed tomography the specimen is exposed for a certain time and the local absorption coefficient is calculated for different rotation steps of the specimen [Ref 44]. As cited from [Ref 44, 45], tomography enables us to start from the total absorption along a set of rays through the specimen and find the local absorption coefficient in small volumes. It does this from a set of exposures at different angles through the same volume element and using Fourier analysis. Roughly speaking, one is able to "average out" the contributions of intervening materials by looking from all angles.

A typical computed tomography setup consists of an X-ray source, collimator, specimen stage, detector or screen and a computer to store the tomograms and to reconstruct them to form the 2D cross-sectional images. There are two methods to scan a specimen which

is placed in between the source and the detector. One method is being rotating the source-detector setup keeping the specimen constant. In this method the source and the detector setup are rotated at a fixed rotation step and the images for all scans are collected for each of these steps. This principle is generally used in the medical scanners called as Computerized Axial Tomography (CAT) scanner. On the other hand, the source-detector setup is kept constant with the specimen stage being rotated for a fixed rotation step in the second method. This method is used generally in the material science field to scan the internal structure of the materials of interest.

The specimen is placed in between the source and the detector and X-rays are passed through the specimen. Depending upon the absorption of the X-rays by the specimen the detector measures the total radiation reached through a slice/cross-section of the specimen. By using the above NDT technique we can detect the internal structure and flaws in composite materials which is of interest in this research work.

4. Experimental Set-Up and Procedure

The main intention of this experimental work is to calculate the microcrack density at different stress levels in three different composite material systems. As described by Nairn [Ref 27], a logical experiment to characterize the microcracking properties of composite laminates is to follow the microcracking process and record the number of microcracks or microcracking density as a function of applied load. Hence our aim in this experimental work is to determine the microcrack density as a function of applied load.

This experimental work consists of five parts, 1) preparation of the test samples, 2) tensile loading of the samples to different stress levels, 3) dye penetration into the loaded sample to make the cracks and damage show prominently, 4) investigation for edge cracks in the samples using optical microscopy and 5) investigation of microcracks in the samples using X-ray microtomography.

4.1 Material System and Sample Preparation

The carbon-epoxy cross ply composite panels which were used in the experimental work were made of three different resin systems. These three different panels have the same lay-up [90/0/0/90] with different material systems. IM7/977-2, IM7/5555, and IM7/5276-1, are the panels which were used, where IM7 are the fibers and 977-2, 5555 and 5276-1

are the three different resin systems. 30 cm x 30 cm composite panels were manufactured by vacuum bagging at the Lockheed Martin Space Systems Company - Michoud Operations. Prior to cutting, these panels were tested via ultrasonic testing and concluded that they posses no initial damage. Each panel had four plies with [90/0/0/90] lay-up. Thickness of each panel varied with IM7/977-2 being 0.55 mm, IM7/5555 being 0.55 mm, and IM7/5276-1 being 0.60 mm.

Samples have been cut from each of the panels with 0deg plies on the outside and 90deg plies in the inside using a diamond cutter. The blade of the cutter is a diamond metal bonded, wafering blade. The panels being big, they were given an initial cut so that they fit on the cutting machine to shape into the required dimensions. These initial cuts were made using a table saw with tape on the composite panel to get proper and smooth cut without inducing damage to the composite material.

After the initial cut each panel was cut into 16 pieces with approximately 7.5 cm x 7.5 cm dimensions. Now from the above 7.5 cm x 7.5 cm piece, test samples were cut down to the dimensions of 50 mm x 5 mm (height x width). These dimensions are required for the sample to accommodate both the tensile loading apparatus and the X-ray microtomography machine. The main intention of the experiments is to conduct tensile tests on the samples and then count the number of cracks induced at different stress levels. Before applying tensile load, the samples were adhered with tabs on both sides at the ends. These tabs protect the sample from crushing because of the stress concentrations caused by the grip of the jaws and also these tabs provide a smooth

gripping surface. Tabs distribute gripping stress and prevent them from crushing. Tabs were cut from an aluminum metal sheet of 0.82 mm thickness and glued to the sample as shown below in Figure 4.1. The dimensions of the tabs are 12.5 mm x 5 mm. These length and width dimensions of the tabs are determined based on the grip area of the clamps of the tensile test machine. These tabs were glues on the either sides of the test sample with the total area exposed to tension being 25mm in height.

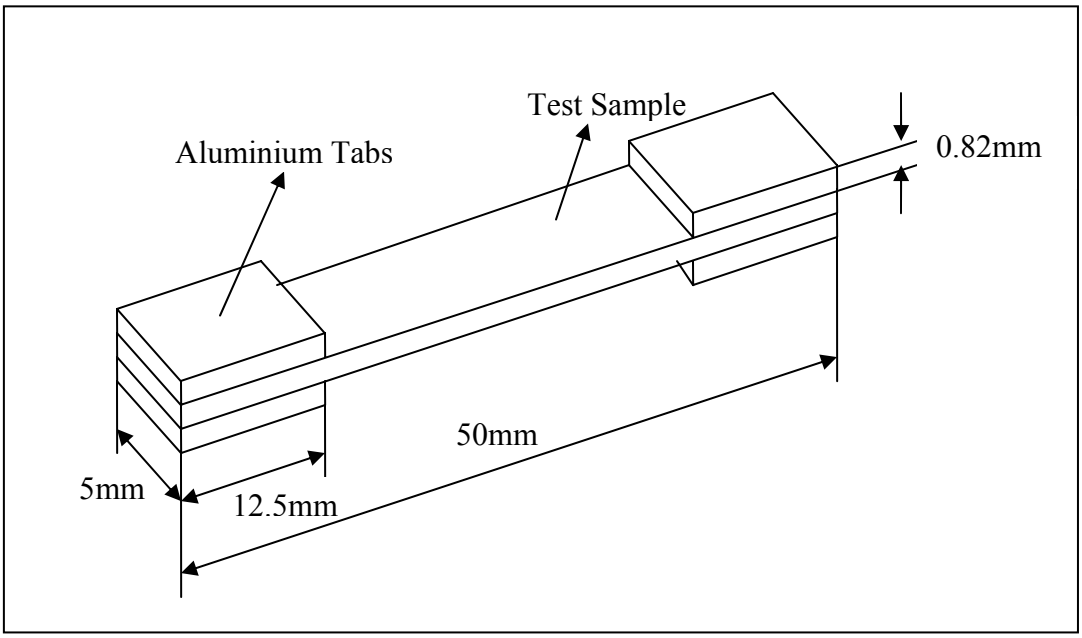

Figure 4.1 *Schematic of typical test sample*

4.2 Tensile testing

Each of the test samples (50 mm x 5 mm dimensions) was loaded on a small tensile sub-stage which has a load cell that can apply loads up to 1000 lbs (4450 N). Uni-axial tension was applied to the sample as shown in the Figure 4.2. Samples from three different panels with three different material systems were loaded to different stresses in

an increasing order. Initially, one sample from each material system was tested to failure to determine the failure stress or the maximum stress that can be applied to the rest of the samples of that material system. Then predetermined incremental loads were applied to the rest of the samples taking into account that these samples were not stressed to failure. The idea behind these predetermined incremental loads is to record the number of microcracks induced at a particular stress level using the X-ray tomography machine.

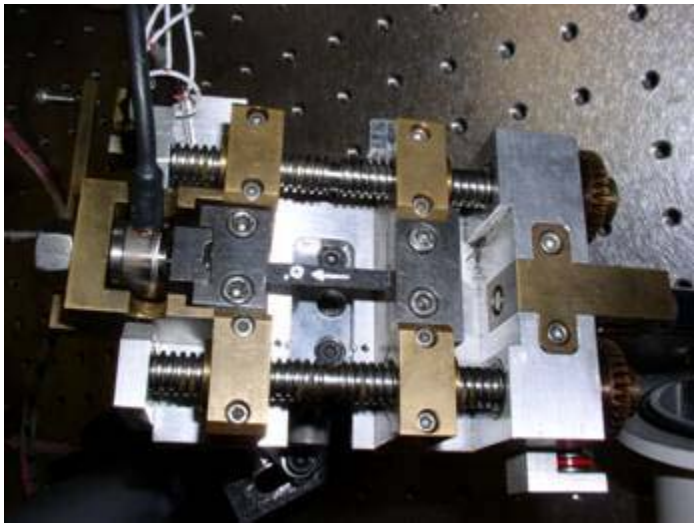

Figure 4.2 *Tensile sub-stage loaded with a composite sample.*

4.3 Dye penetration

The X-ray microtomography machine works mainly on the contrast differentiation in the sample. So in order to get better contrast between the cracks and the matrix material we used a dye penetrant as the medium to enhance the cracks by making them more visible in the radiography. The use of specialized penetrants in the field of composite materials was first described by Crane [Ref 46]. The dye which we used was made of isopropyl alcohol (5 ml), zinc iodide (30 gms), Kodak photo solution (5 ml) and distilled water (5

ml). The samples were then soaked in this dye for about 5 hours which gives the dye enough time to penetrate into the crack opening and make them more visible in the radiography pictures. The use of dye penetrant to enhance the microcrack visibility in the graphite/epoxy composite materials was also suggested by Bhanu Karedla [Ref 47]. His study shows that dye penetrated through the microcracks and when the sample soaked in this dye was viewed in the X-ray tomography instrument, the cracks were more prominently visible than in the sample with no dye.

4.4 Optical Microscopy

After the cracks were tensile tested and soaked in the dye penetrant, they were examined for the edge cracks under an optical microscope. The main intention of using this optical microscope is to record the number of edge cracks on both sides of the test sample and to find the surface flaws like matrix cracking, voids and surface delaminations if any. By comparing these number of edge cracks to the number of cracks measured through the X-ray tomography we can say whether these cracks are all the way through the width of the sample or not. This edge crack recording by optical microscopy also provides us a comparison to verify the X-ray microtomography results.

4.5 Investigation of Microcracks Using X-Ray Microtomography

As discussed in chapter 3, X-ray microtomography is a non-destructive technique used to get the high resolution images of the internal microstructure of the material of interest. The use of X-ray microtomography to detect internal damage in fiber reinforced polymer matrix composites was also demonstrated by Bhanu Karedla [Ref 47].

4.5.1 Details of Skyscan 1072

The X-ray microtomography experiments were carried out using a Skyscan 1072 compact desktop system. The typical details about this Skyscan microscanner are gathered from the instrument manual. The equipment contains an X-ray microfocus tube which can operate at high voltage power supply of 20-100kV / 0-250μA with a maximum power of 10W. A specimen stage with precision manipulator including two translations and one rotation is available. Translations being 1) movement along the optical axis to zoom in or zoom out 2) lowering and rising of the sample stage to scan the required area of interest along the length of the sample. Rotation being 180º/360º with 0.45º/0.68º/0.90º rotation step.

The X-ray detector consists of an X-ray scintillator which is fiber optically coupled (3.7:1 image reduction) to a high resolution (1024x1024 pixels) cooled CCD camera. The CCD camera is connected to a frame grabber to record the X-ray shadow projections which are digitized to 1024x1024 pixels with 4096 brightness gradations (12 bit). These projections are recorded in TIFF format to the digital frame grabber. The reconstruction of the data consists of acquiring the X-ray images from 200 to 400 rotation views over 180 or 360 degrees of sample rotation.

A con-beam reconstruction algorithm is used to perform the reconstruction by the X-ray microtomography machine. Serial reconstructions of cross-sections are carried out using the cone-beam reconstruction algorithm. These reconstructed cross-sections can be viewed on the screen and can be used to construct a realistic 3D model of the sample by

using the 3D creator. This software facilitates building the 3D model of the sample with features to rotate and cut the sample model. The computer used to carry out all the above functions is a Dell Precision 420, with Pentium 4 – 2GHz processor, 1.047 GB RAM, 102 GB Hard Disk and working on Windows 2000 Professional operating system.

4.5.1.1 Calibration of Skyscan 1072

Prior to the start of experimental work, the Skyscan 1072 system must be calibrated to get the correct results. Two basic things to calibrate the system are flat field correction and an alignment test. Flat field correction is used to acquire illumination irregularities of the X-ray tube and the camera sensitivity map. In the flat field correction we acquire and save the reference field without any sample but with the same acquisition parameters used to scan a sample. An alignment test of the system is required to correctly align the camera and the X-ray tube. This alignment test also shows the displacement of the sample rotation axle from the ideal position.

4.5.1.2 Optimization of Scan Parameters of Skyscan 1072

To detect microcracks using this X-ray microtomography machine, it is necessary to determine and optimize the scanning parameters required to obtain the desired information of the microcracks both qualitatively and quantitatively. Several important parameters to be optimized are

1) Rotation step or the angular increment given to the sample stage during the scan.

2) Voltage, which determines the energy of the X-rays and

3) Power, which determines the spot size of the X-ray source.

A detailed procedure about optimization and experimental verification was presented by Bhanu Karedla in his thesis [Ref 47]. From his work it was concluded that a rotation step of 0.90º, high voltage 100kV and high power 10W are recommended to be the good scan parameters.

4.5.2 Experimental Procedure

A step by step procedure, right from loading the sample on the sample stage to creating 3D images using X-ray microtomography was given by Bhanu Karedla [Ref 47]. These steps include:

1) Loading of the sample on the sample stage.

2) Aligning the axis of the sample with that of the sample stage to make sure the image of the sample is within the screen while rotating the sample.

3) Switching on the X-rays for experimental work.

4) Adjusting the magnification to make sure that the image of the sample is within the screen while rotating the sample.

5) Setting the parameters like rotation step and total rotation angle for the experiment.

6) Adjusting the voltage and power to get good image of the sample.

7) Setting the exposure time for getting good scanned image of the sample.

8) Checking the intensity graph of the 2D X-ray image to make sure that there is enough contrast between the sample and the medium in the 2D X-ray image.

9) Acquisition of the 2D X-ray images in the TIFF format. By using this command the images are acquired for each rotation step of the sample. So if we have 180º / 0.9 º rotation steps, then all together we get 200 2D X-ray images for the sample.

10) Reconstruction of the cross-sections. By using this command we can either reconstruct one single cross-section or a group of cross-sections from the existing TIFF files. After reconstruction we can view each and every cross-section of the sample in its top-view.

11) 3D modeling of the sample is done using the 3D-Creator program. By creating the 3D model of the sample we can view the internal structure and defects contained by that sample.

By following the above step by step procedure the experiments were performed on the samples from the three different composite material systems which were tensile tested to different stress levels and soaked in dye-penetrant for a time period of 5 hours. They were approximately 14 samples from each of the three different material systems and the above procedures have been followed to scan the samples for microcracking. All the scanned data from each of the sample was stored carefully for further investigation of microcracks and other possible defects.

4.5.3 Data from the X-ray Microtomography

Many large data files are generated from the tomography machine from acquisition to 3D model creation. As an example, images of one of the samples from the composite material system IM7/5555 are shown below. This material system consists of [0/90/90/0] configuration. A typical 2D X-ray image or radiograph of the front view of the sample would look like the one shown in Figure 4.3 and the 2D X-ray image or radiograph of the side view of the sample is shown in Figure 4.4. In the figures we can see only a partial

portion of the sample in the vertical direction; this is called the field of view. This portion of the sample is right in-between the tabs and is approximately 9.32mm in height of the sample at x30 magnification. The field of view of the sample depends on the magnification. At low magnification we have larger field of view and at higher magnification we have smaller field of view. Field of views at different magnifications is listed below in Table 4.1 as measured from the tomography instrument.

Magnification	**Pixel (µm)**	**Field of View (mm x mm)**
X14	19.05	19.493x19.493
X20	13.67	13.986x13.984
X30	9.11	9.324x9.324
X40	6.84	6.994x6.994
X50	5.47	5.593x5.593
X60	4.56	4.661x4.661
X70	3.91	3.992x3.992
X80	3.42	3.494x3.494
X90	3.04	3.107x3.107
X100	2.73	2.796x2.796
X110	2.48	2.542x2.542

Table 4.1 *Field of view at different magnifications*

In Figures 4.3 and 4.4 we can see the actual window of the Skyscan software with all the icons and menu items which are used to scan the sample and get the required information. We can also see the scanning parameters of the machine on the extreme right side of the window, which shows parameters like magnification, pixel size, voltage and current of the source, lift of the sample, rotation step and exposure. In the figures below we can see the microcracks in the sample in both the front and side view of it. We can see a total of four microcracks in the field of view of which three of them are running all the way through the width of the sample and one runs only half way through the width starting from one edge.

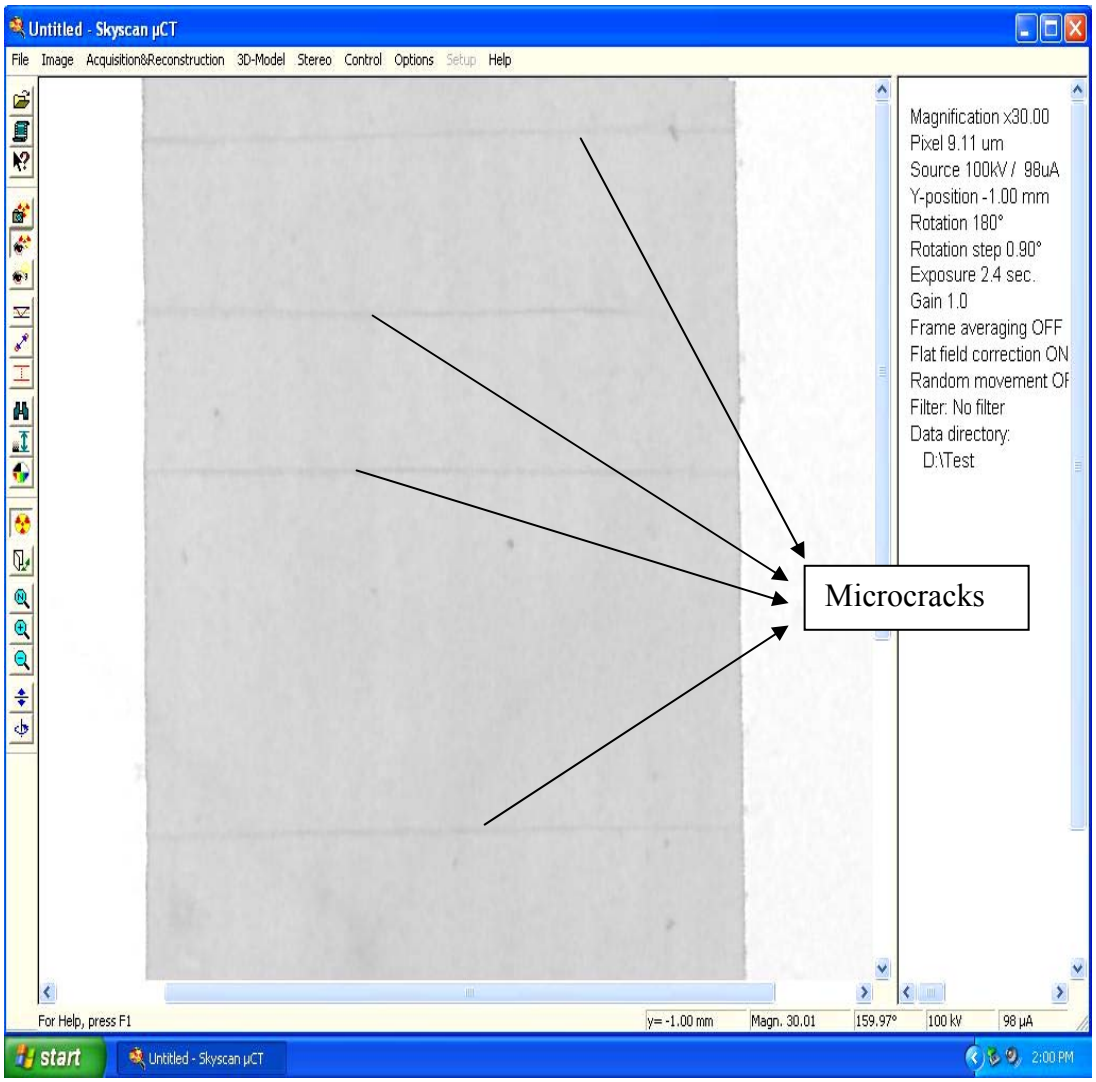

Figure 4.3 *Two Dimensional X-ray image of sample in the front view*

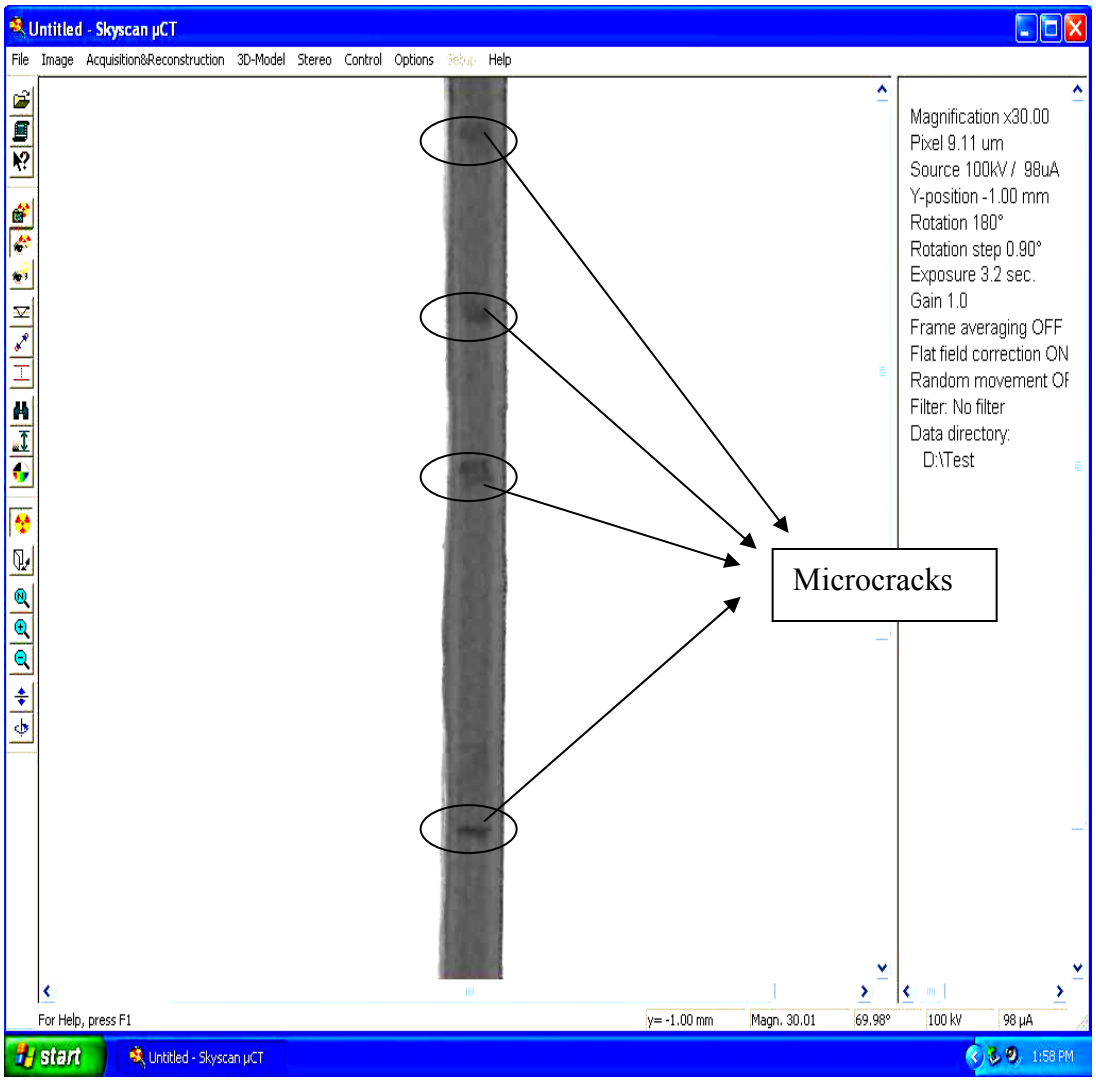

Figure 4.4 *Two Dimensional X-ray image of sample in the side view*

In Figures 4.3 and 4.4 we can see only a partial portion of the sample which is in between the tabs. By following the experimental procedure which was stated above, acquisition and reconstruction of the sample were performed. After reconstruction we have the cross-sectional images of the sample. The top view of one such cross-sectional image of the sample is shown in Figure 4.5. In this cross-sectional view we can see the thickness and width of the sample which are marked on the image. A number of such cross-sectional

images will be constructed from the acquisition data. Typically we can construct 1000 cross-sectional images right from top to bottom of the portion of the sample visible on the screen, i.e., field of view of the sample.

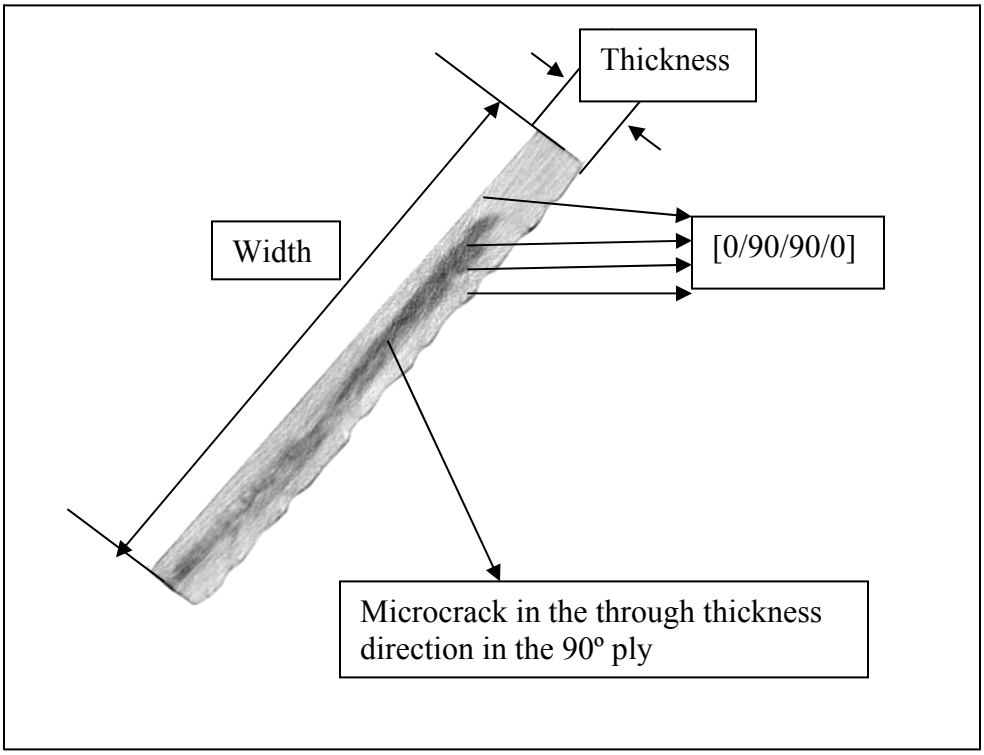

Figure 4.5 *Cross-sectional image of the sample with microcrack*

In the cross-sectional image shown in Figure 4.5 we see that dark region in the middle layer of the sample along the thickness. This is the microcrack which extends all the way through the thickness in one of the cross-section of the sample. Because the dye which was used in the experiment is denser than the composite material, this shows that the dye has penetrated through the microcrack and shows up as dark region in the cross-sectional view. Now with the above cross-sectional images the 3-Dimensional image was constructed and is shown in the Figure 4.6.

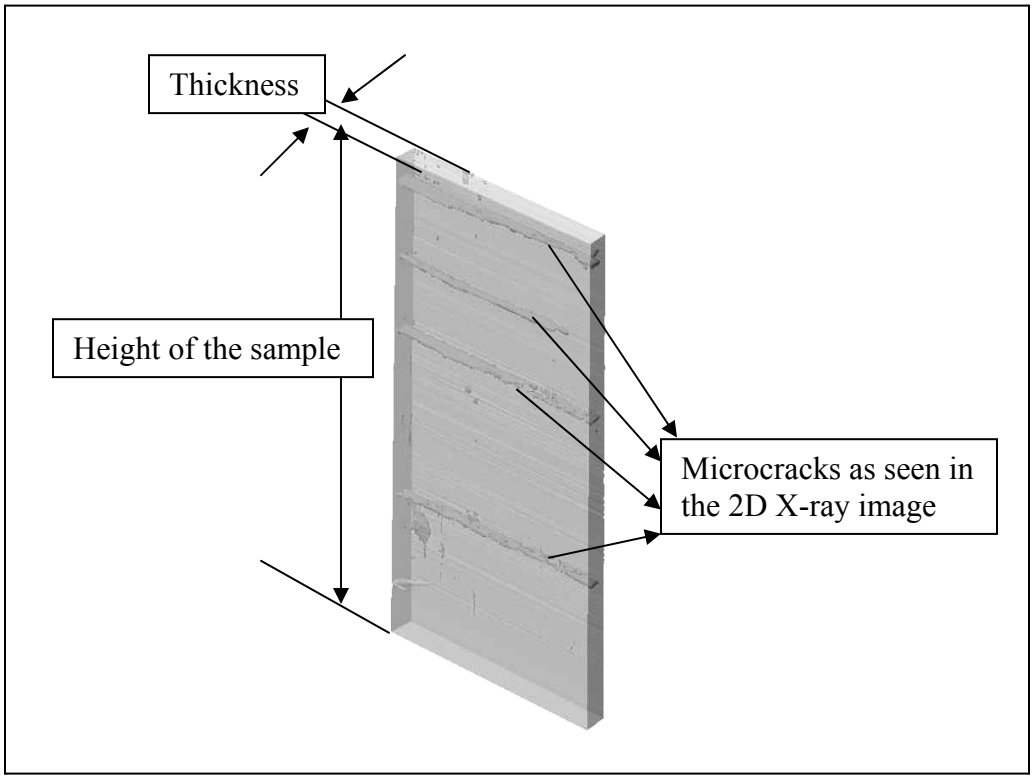

Figure 4.6 *Three-Dimensional image of the sample*

In the 3D image shown in Figure 4.6 we can see four microcracks out of which three run all the way through the width of the sample and one runs only half way starting from one edge. The same observation was made from the 2D X-ray images of the sample. Hence by using the 3D image construction we can get the same information as we have seen in the 2D X-ray image. To know more details about the damage we now can rotate the 3D image to different views to know how far the microcracks are running in the thickness direction and is there any other form of damage other than only the microcracks, like delamination and etc. In this way damage types can be determined using the 3D image which cannot be inferred from the 2D images. With the above knowledge of experimental

procedure and image acquisition we now proceed to the next chapter to discuss the results which were obtained.

5. Results and Discussions

By following the above experimental procedures we get the 2D and 3D images and from these images we need to interpret the required information. These experimental procedures were followed for scanning the three composite material systems IM7/977-2, IM7/5555 and IM7/5276-1. From the 2D X-ray images the microcracks were counted to determine the microcrack density which is of primary interest for the experimental work and from the 3D image the types of damage and damage connectivity were inferred.

5.1 Microcrack Density

The entire height of the sample (50 mm) did not fit within the field of view at the predetermined magnification x30. Therefore, the sample was lowered and raised in order to count the total number of microcracks which are induced in the region between the tabs (approximately 25mm). Microcrack density is calculated by dividing the number of microcracks formed by the length of the region over which they are formed. This microcrack density is very important to the finite fracture mechanics field in determining the fracture toughness and to validate the formulations made for critical strain release rate. The results for $[0/90]_s$ laminates for the three material systems are presented in the following three sections.

5.1.1 Composite Material System IM7/977-2

A total of 13 $[0/90]_s$ IM7/977-2 samples were tested to predetermined incremental loads on the tensile substage shown in Figure 4.2. After testing, these samples were soaked in dye penetrant for more than 5 hours each and then scanned for microcracks in the X-ray microtomography machine. The progression of microcrack development was recorded from the 2D X-ray images of each sample. In Table 5.1 different radiographs or 2D X-ray images are shown to illustrate the progression of microcracking with increase in stress on the samples from IM7/977-2 material system.

IM7/977-2 Material System			
1100MPa	**1200MPa**	**1302MPa**	**1400MPa**
			
0.65 cracks/cm	**2.96 cracks/cm**	**8.53 cracks/cm**	**15.08 cracks/cm**

Table 5.1 *X-Ray images of samples from $[0/90]_s$ IM7/977-2 material system. Area of the sample which is seen here is about 9.3mmx5mm*

In Table 5.1 we can see that the microcrack density increases with increase in stress in different samples. The first microcrack was observed to form at 1100MPa of stress and the microcracks increased thereafter as the stress increased. As an example, a 1200MPa six microcracks were observed over the 20.3 mm region between the tabs on the sample, giving a microcrack density of 2.96cracks/cm. A plot of the microcrack density as a function of the applied stress is shown in Figure 5.1 for IM7/977-2 material system. In this plot we can see the increase in microcrack density with the stress.

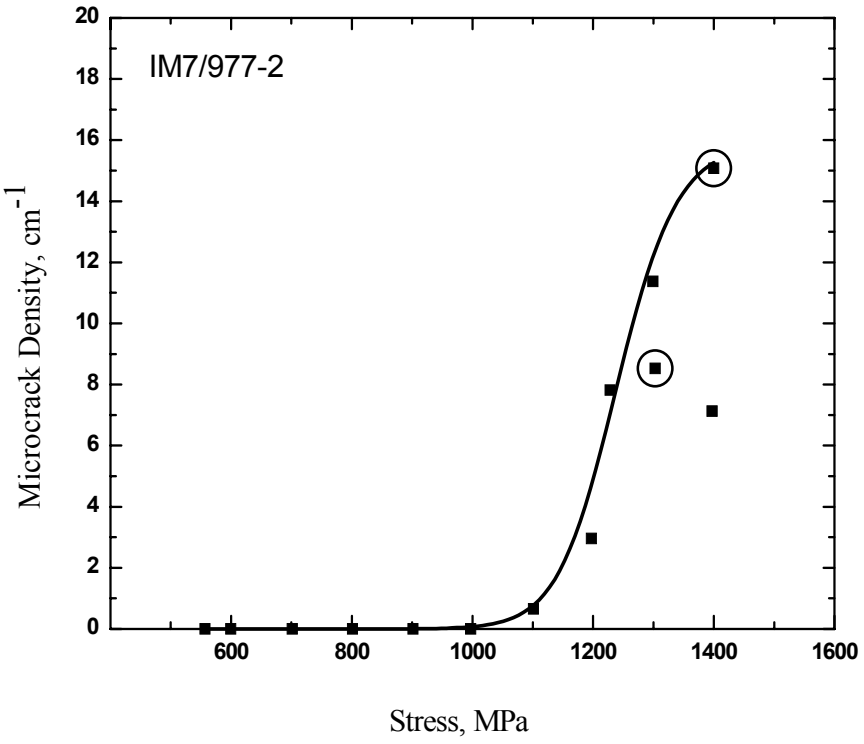

Figure 5.1 *Microcrack Density vs. Stress Plot for* $[0/90]_s$ *IM7/977-2*

As seen from the crack density plot, the onset of microcracking was observed to form at around 1100MPa of stress with less than one crack per centimeter. Thereafter the number

of microcracks increased with increase in stress. It was observed that there was a steep increase in microcrack density when compared to the stress. The microcracks were observed to form almost instantaneously across the length of the sample. As observed from the above experiments the crack density saturation was determined to be around 15 cracks per centimeter. The data points marked with circles in the crack density plot represent specimens in which the material failed. The failure stress for this IM7/977-2 material system was determined to be between 1300MPa and 1400MPa. We can see that there were two samples tested to 1400MPa, one of them failed and the other showed low crack density at the same stress. This might be because of two reasons, one being the improper gripping of the jaws because of poor adhesion of the tabs and the other being inaccuracy in maintaining constant cross-sectional area for the samples.

Until the stress reached around 1300MPa the microcracks were found only in the 90º plies, but as the stress reached 1302MPa, microcracks were observed even in the adjacent 0º plies. These cracks were seen running parallel to the load direction and along the fibers in the outer 0º plies, i.e., the cracks in the outer 0º plies run perpendicular to the cracks in the 90º plies. At 1302MPa and 1400MPa delamination was observed in between the adjacent plies followed by longitudinal fiber splitting which lead to overall failure of the sample.

5.1.2 Composite Material System IM7/5555

A total of 16 $[0/90]_s$ IM7/5555 samples were tested to predetermined incremental loads on the tensile substage shown in Figure 4.2. After testing these samples were soaked in

dye penetrant and then scanned for microcracks. In Table 5.2 different radiographs or 2D X-ray images are shown to illustrate the progression of microcracking with increase in stress on the samples from the IM7/5555 material system.

IM7/5555 Material System			
800MPa	**1000MPa**	**1200MPa**	**1300MPa**
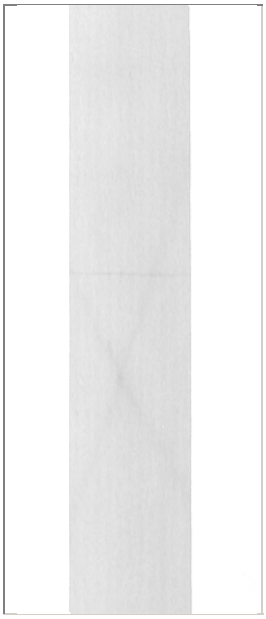	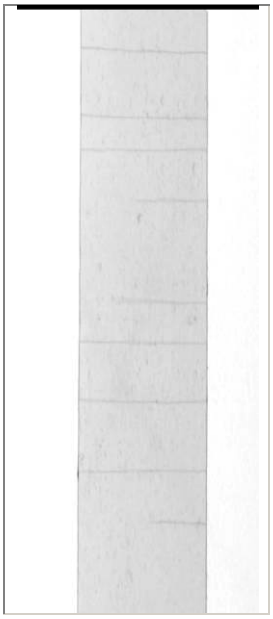	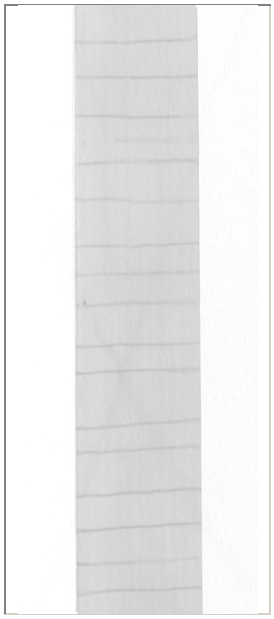	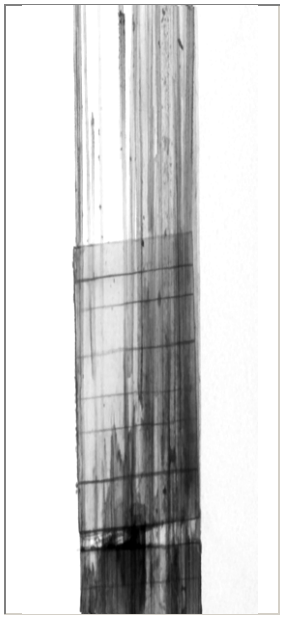
1.02 cracks/cm	**9.52 cracks/cm**	**16.26 cracks/cm**	**No count**

Table 5.2 *X-Ray images of $[0/90]_s$ samples from IM7/5555 material system. Area of the sample which is seen here is about 9.3mmx5mm*

At 1300MPa the material IM7/5555 failed completely as can be seen in the Table 5.2. The microcrack density was calculated for each sample and a plot of the microcrack density as a function of the applied stress is shown in Figure 5.2. In this plot we can see the increase of microcrack density with the stress.

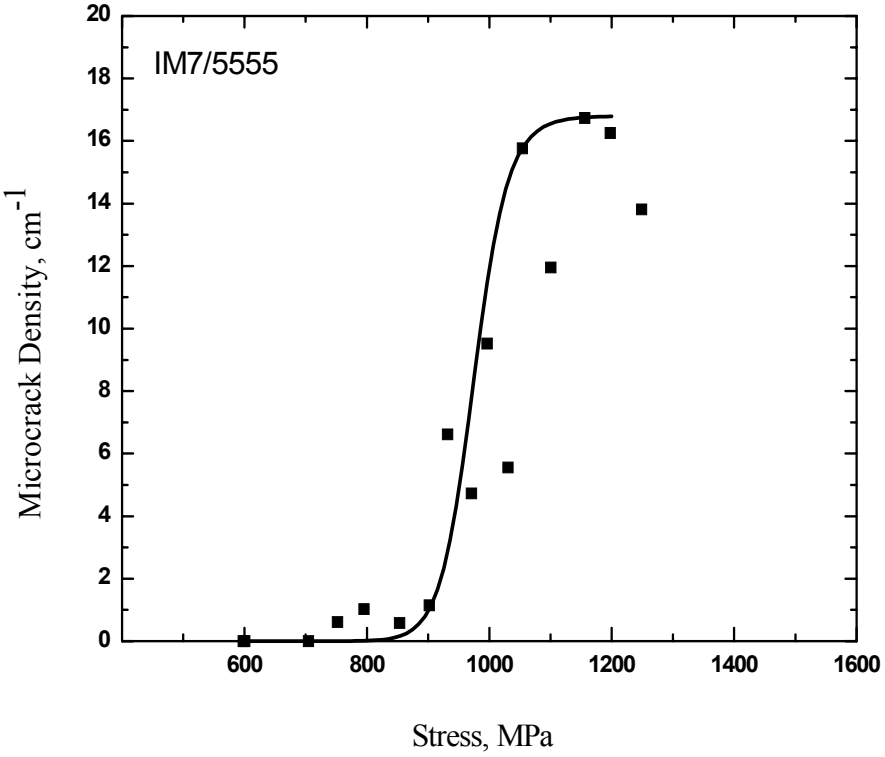

Figure 5.2 *Microcrack density vs. Stress Plot for* $[0/90]_s$ *IM7/5555*

The onset of microcracking was observed at around 750MPa stress level with one crack per centimeter. Thereafter the number of microcracks slowly increased with increase in stress. From the crack density plot we can see that there is a steep increase in microcrack density when compared to the stress. The microcracks were observed to form almost instantaneously across the whole length of the sample. One observation made from the plot is that the microcrack density tends to saturate before failure for the IM7/5555 material system. This saturation of microcrack density is called as Crack Density Saturation point. The crack density saturation based on observations made from the samples was determined to be approximately 16 cracks per centimeter. We can see that

there are many data points which scattered around the cracks density curve in the plot. This was because of the inaccuracy in maintaining constant cross-sectional area for the samples. The failure point at 1300MPa was not shown in the plot, as the sample failed completely which made it difficult to count the microcracks as can be seen in the radiograph in Table 5.2. Hence the failure stress for the above IM7/5555 material system was observed to be between 1250MPa to 1300MPa.

Until the stress reached to around 1250MPa the microcracks were found only in the middle 90º plies, but as the stress reached above 1270MPa, microcracks were observed even in the adjacent 0º plies. At 1290MPa delamination was observed in between the outer 0º plies and the adjacent 90º plies and the sample failed completely as can be seen in the figure from the above Table 5.2.

5.1.3 Composite Material System IM7/5276-1

A total of 12 $[0/90]_s$ IM7/5276-1 samples were tested to predetermined incremental loads on the tensile substage shown in Figure 4.2. After testing these samples were soaked in dye penetrant for more than 5 hours each and then scanned for microcracks in the X-ray microtomography machine. The progression of microcrack development was recorded from the 2D X-ray images of each sample. In Table 5.3 different radiographs or 2D X-ray images are shown to illustrate the progression of microcracking with increase in stress on the samples from the IM7/5276-1 material system.

IM7/5276-1 Material System			
950MPa	**1000MPa**	**1060MPa**	**1100MPa**
		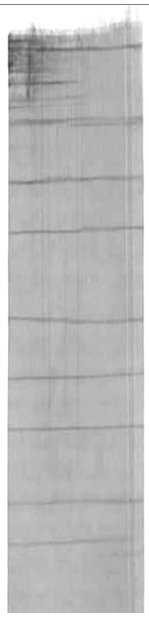	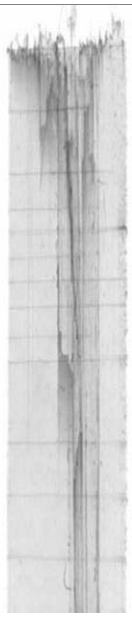
950MPa	**1000MPa**	**1060MPa**	**1100MPa**

Table 5.3 *X-Ray images of $[0/90]_s$ samples from IM7/5276-1 material system. Area of the sample which is seen here is about 9.3mmx5mm*

As can be seen in Table 5.3, the two samples which were stressed up to 1060MPa and 1100Mpa failed, due to delamination and longitudinal fiber splitting. The microcrack density was calculated and the plot for crack density vs. stress is shown in Figure 5.3 for the IM7/5276-1 material system.

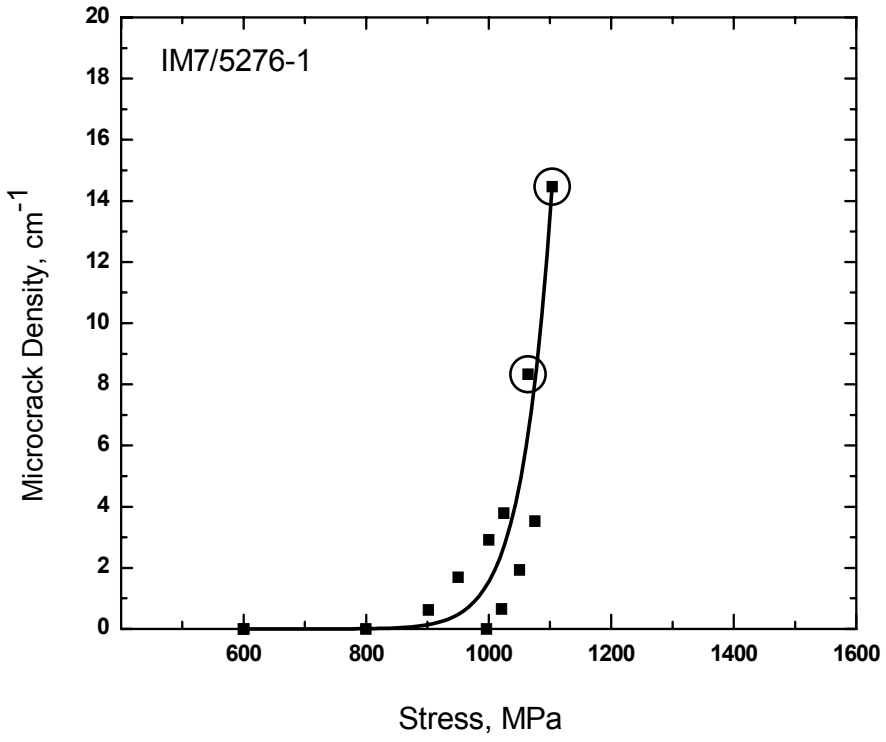

Figure 5.3 *Microcrack Density vs. Stress Plot for [0/90]$_s$ IM7/5276-1*

The onset of microcracking was observed at around 900MPa of stress level with less than one crack per centimeter. There is a steep increase in microcrack density when compared to the stress and the microcracks were observed to form almost instantaneously across the length of the sample. It was observed that the material failed with out showing proper saturation in the crack density and the saturation crack density was observed to be approximately 14.5 cracks per centimeter. It can be seen that there are a few data points which scattered around the cracks density curve and out of the two data points showing failure, one has higher crack density compared to the other. This is because of the inaccuracy in maintaining constant cross- sectional area for the samples.

The data points marked with circles represents specimens for which the material system failed at that particular stress level. Hence it can be observed that the failure stress for the IM7/5276-1 material system is between 1050MPa to 1100MPa.

Until the stress reached to around 1060MPa the microcracks were found only in the 90º plies, but as the stress reached above 1060MPa, microcracks were observed even in the adjacent 0º plies. At this stress delamination was observed in the sample followed by longitudinal fiber splitting which lead to the overall failure as seen in the corresponding figure from Table 5.3. At 1100MPa the sample showed higher crack density and the delamination at this stress level was observed to be on a larger scale when compared to the previous sample (stressed to 1060MPa). This sample failed with lots of delamination and longitudinal fiber splitting in the outer 0º plies.

5.2 X-Ray Microtomography Results

As discussed earlier in chapter 3, X-ray microtomography is an excellent NDT tool for characterizing the three dimensional geometry of defects in composites. By using X-ray microtomography in this research the development of microcracking and other forms of damage were investigated. Primarily, microcracking is the first phase of damage which was investigated followed by delamination and fiber splitting. Initially in all the three material systems, microcracks were observed in the early stages along the 90º plies and as the stress increased, cracking of the outer 0º plies was observed and other forms of damage like delamination and fiber splitting followed them at higher stress levels.

Samples from three different material systems were investigated and the results are shown in the figures below.

5.2.1 Material System IM7/977-2

Samples from $[0/90]_s$ IM7/977-2 laminates were examined for microcracking and other forms of damage at different stress levels. At higher stresses delamination and longitudinal fiber splitting were observed and this can be observed clearly in the 3D models obtained from the X-ray tomography results.

3D models of the IM7/977-2 samples tested to 1298MPa and 1400MPa are shown in Figure 5.4 and Figure 5.5. In these models we can see a portion of approximately 7.5mm x 5mm of the sample. From these 3D models it can be observed that the progression of microcracking increases with increase in stress. It was observed that the microcracks in the middle 90º plies were formed in both these samples, but the cracking of the outer 0º plies could be seen only in the 1400MPa sample and this sample failed due to delamination and fiber splitting. The cracking of the outer 0º plies for the IM7/977-2 samples tested, occurred at the failure stresses and the sample failed showing delamination and fiber splitting. There was no sufficient data from the tested samples to determine the onset of cracking in the outer 0º plies.

In Figure 5.4 we can see microcracks in the middle 90º plies and in Figure 5.5 microcracks were formed in the middle 90º plies and cracking of the outer 0º plies was also observed. This sample tested to 1400MPa failed due to delamination and fiber

splitting which is shown in the Figure 5.5. Delamination is observed in between the 0º and 90º plies and longitudinal fiber splitting of the outer 0º plies is seen in Figure 5.5. The microcracks in the 90º plies of the sample in Figure 5.4 correspond to crack density of 11.4 cm^{-1} and the sample in Figure 5.5 correspond to crack density of 15 cm^{-1} as shown in Figure 5.1. In creating the 3D models the matrix material model was given a high level of transparency and the microcracks were artificially rendered color to visualize them more clearly.

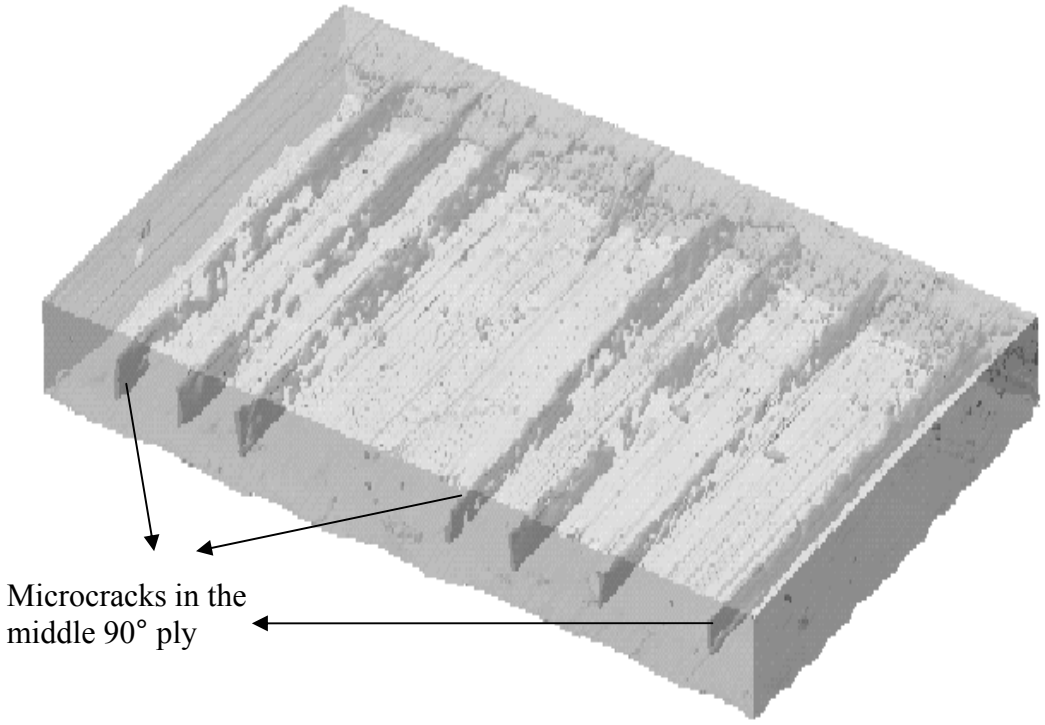

Figure 5.4 *Three Dimensional Model of Sample from IM7/977-2 loaded to 1298MPa*

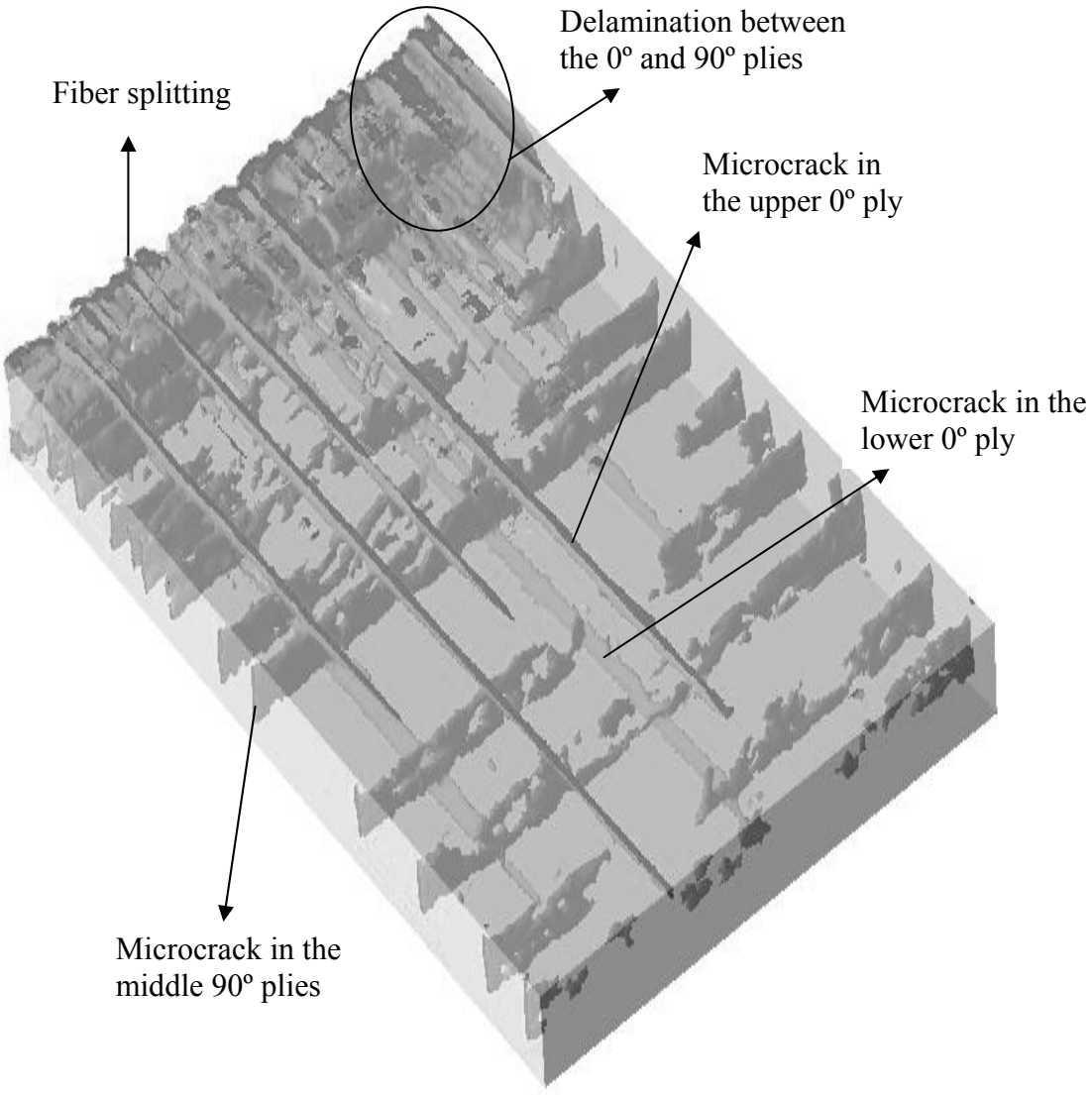

Figure 5.5 *Three Dimensional Model of Sample from IM7/977-2 loaded to 1400MPa*

In Figure 5.6 we can see a similar 3D model of sample from the same IM7/977-2 material system loaded to 1302MPa. This sample failed even when the stress is low compared to 1400MPa and the data point of this sample does not follow the trend of the graph shown in Figure 5.1. This may be because of improper adhesion of the tabs or inaccuracy to maintain constant cross-sectional area of the sample.

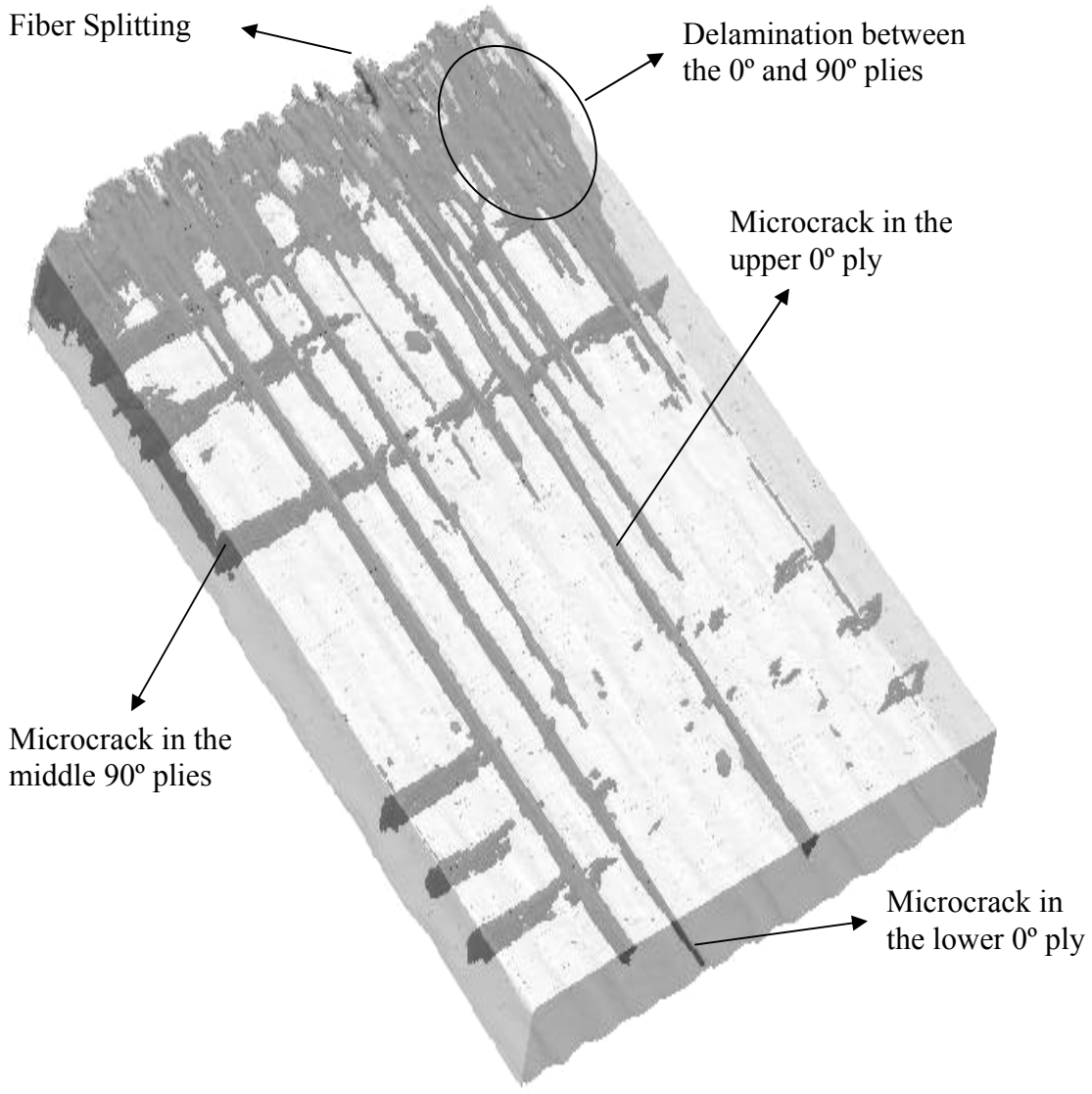

Figure 5.6 *Three Dimensional Model of Sample from IM7/977-2 loaded to 1302MPa*

In the model in Figure 5.6 we can see a portion of approximately 7.5mm x 5mm of the sample. The microcracks in the 90º plies of this sample correspond to crack density of 8.5 cm^{-1} in Figure 5.1, which is less than the crack density (12 cm^{-1}) incurred by the sample stressed to 1298MPa. At this stress level of 1302MPa, it was observed that microcracks formed in the middle 90º plies and the material failed following cracking in the 0º plies with delamination and fiber splitting.

5.2.2 Material System IM7/5555

Samples from $[0/90]_s$ IM7/5555 laminates were examined for microcracking and other forms of damage at different stress levels. At higher stresses delamination and longitudinal fiber splitting were observed and this can be observed clearly in the 3D models obtained from the X-ray tomography results.

From the 3D models shown in Figure 5.7 and Figure 5.8 we can observe the progression of microcracking increases with increase in stress level. A 3D model of the IM7/5555 sample tested to 1250MPa is shown in Figure 5.7. In this model we can see a portion of approximately 7.5mm x 5mm of the sample. Microcracks were observed in the middle 90º plies of the sample at this stress level. The microcracks in the 90º plies of this sample correspond to crack density of 13.8 cm^{-1} in Figure 5.2.

In creating the 3D model the matrix material model was given a high level of transparency and the microcracks were artificially rendered color to visualize them more

clearly. In the figure below we can see voids in the sample which are not clearly visible in the 2D X-ray image of this sample. There are two voids in the model shown with one being an air trap and the other being delamination which is probably due to weak bonding between adjacent layers. This type of delamination was discussed in Chapter 2.

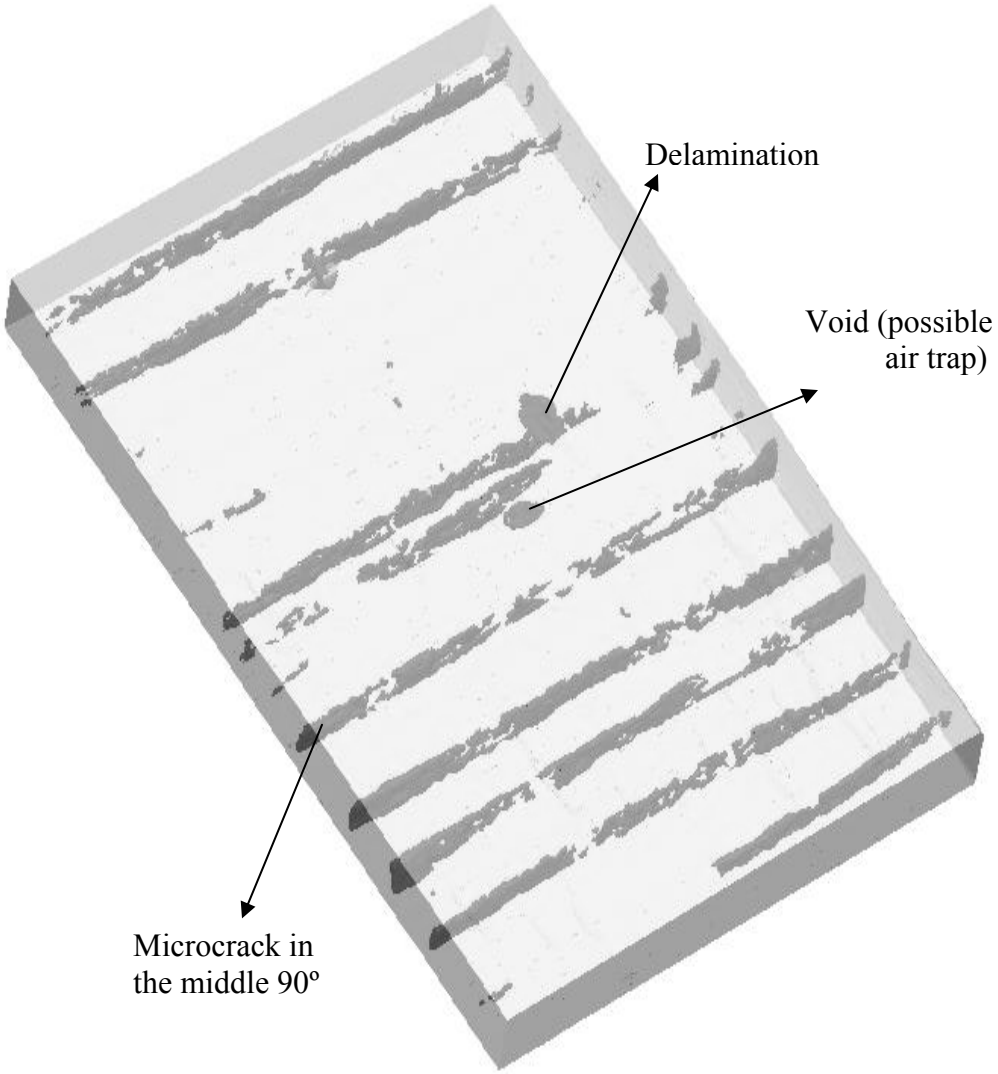

Figure 5.7 *Three Dimensional Model of Sample from IM7/5555 loaded to 1250MPa*

In Figure 5.8 we can see a similar 3D model of a sample from the same IM7/5555 material system loaded to 1280MPa. At this stress level it was observed that a higher number of microcracks formed in the middle 90º plies and the material failed following microcracks in the 0º plies along with delamination and fiber splitting. In the model below we can see a portion of approximately 8.5mm x 5mm of the sample. At this stress level a higher number of microcracks were formed in the 90º plies and only a few 0º ply cracks were observed which lead to delamination and fiber splitting.

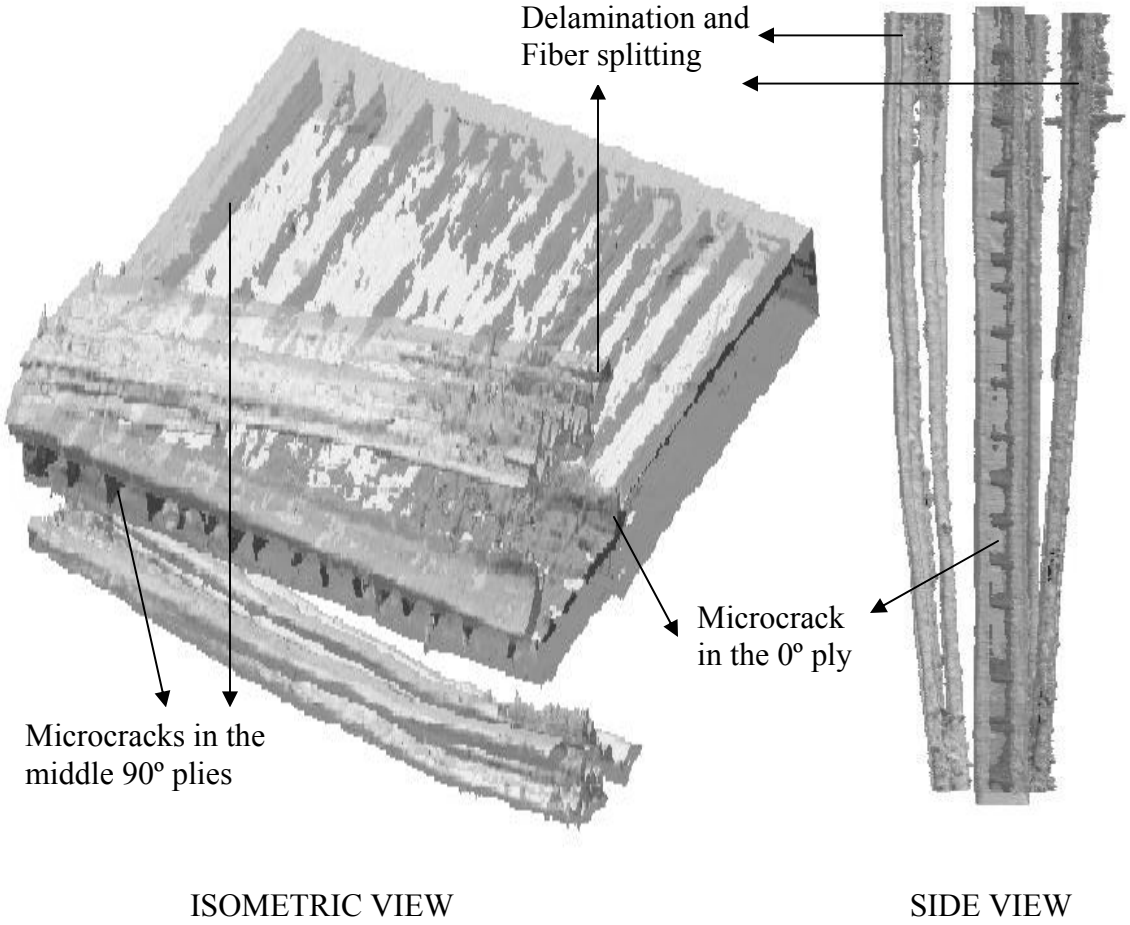

Figure 5.8 *Three Dimensional Model of Sample from IM7/5555 loaded to 1280MPa*

In Figure 5.8 we have two views of the same sample, one in isometric and the other in side view. In both the directions we could see the microcracks in the outer 0º ply along with delamination and longitudinal splitting of the fibers. Delamination between the 0º and 90º plies and longitudinal fiber splitting of the outer 0º plies was observed.

It was observed that the $[0/90]_s$ IM7/5555 material system showed few outer 0º ply cracks. Delamination is observed in Figure 5.7 without the presence of cracks in the 0º plies, and few cracks are observed in these outer plies, even at failure. The cracking of the outer 0º plies was not observed until 1250MPa and at 1280MPa the sample showed few 0º ply cracks and failed due to delamination and fiber splitting. This material system displayed greater resistance to cracking in the outer 0º plies.

5.4.3 Material System IM7/5276-1

Samples from $[0/90]_s$ IM7/5276-1 laminate were examined for microcracking and other forms of damage at different stress levels. At higher stresses delamination and longitudinal fiber splitting were observed and this can be observed clearly in the 3D models obtained from the X-ray tomography results.

3D models of the IM7/5276-1 samples tested to 1020MPa and 1060MPa are shown in Figure 5.9 and Figure 5.10. In the model in Figure 5.9 we can portion of approximately 4.5 mm x 5 mm of the sample and in Figure 5.10 we can see a portion of approximately 7.5mm x 5mm of the sample. From these 3D models it can be observed that the

progression of microcracking increases with increase in stress. It was observed that the microcracks in the middle 90º plies were formed in both these samples, but the cracking of the outer 0º plies could be seen only at 1060MPa and the sample failed due to delamination and fiber splitting. So the onset of cracking of the outer 0º plies occurred at stress levels between 1020MPa 1060MPa.

The sample tested to 1060MPa failed due to delamination and fiber splitting which is shown in the Figure 5.10. Delamination is observed in between the 0º and 90º plies and longitudinal fiber splitting of the outer 0º plies is seen in Figure 5.10. The microcracks in the 90º plies of the sample in Figure 5.9 correspond to crack density of 3.8 cm^{-1} and the sample in Figure 5.10 correspond to crack density of 8.3 cm^{-1} as shown in Figure 5.3. In creating the 3D models the matrix material model was given a high level of transparency and the microcracks were artificially rendered color to visualize them more clearly.

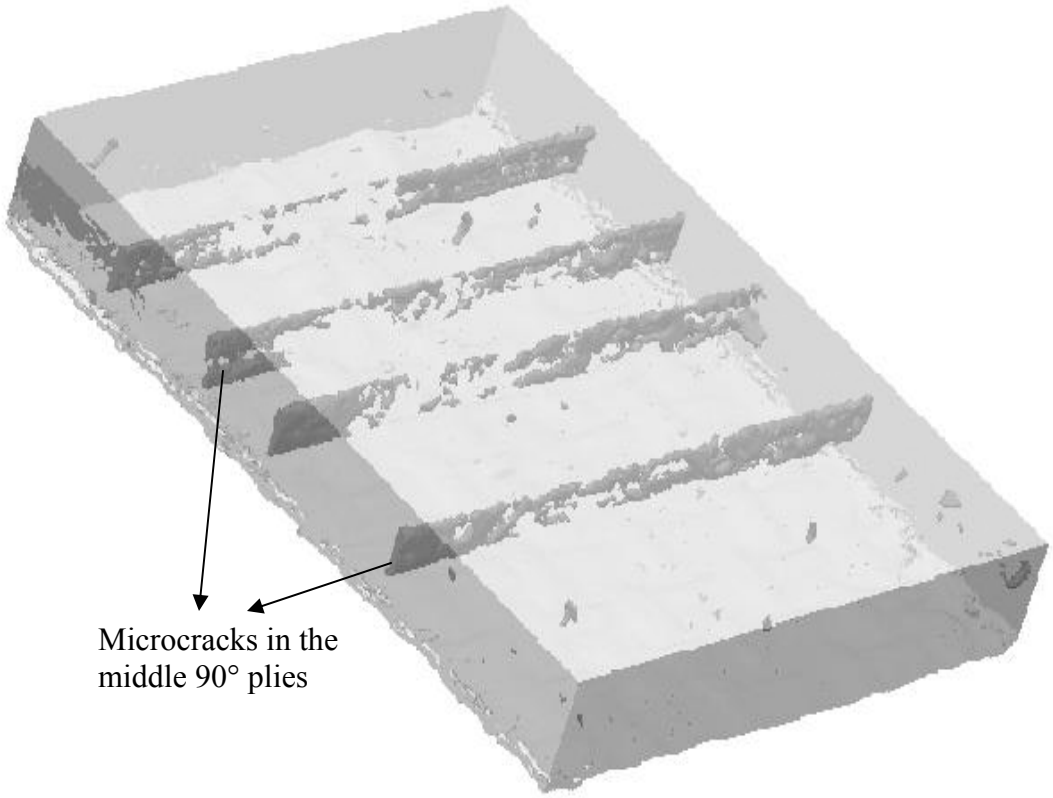

Figure 5.9 *Three Dimensional Model of Sample from IM7/5276-1 loaded to 1020MPa*

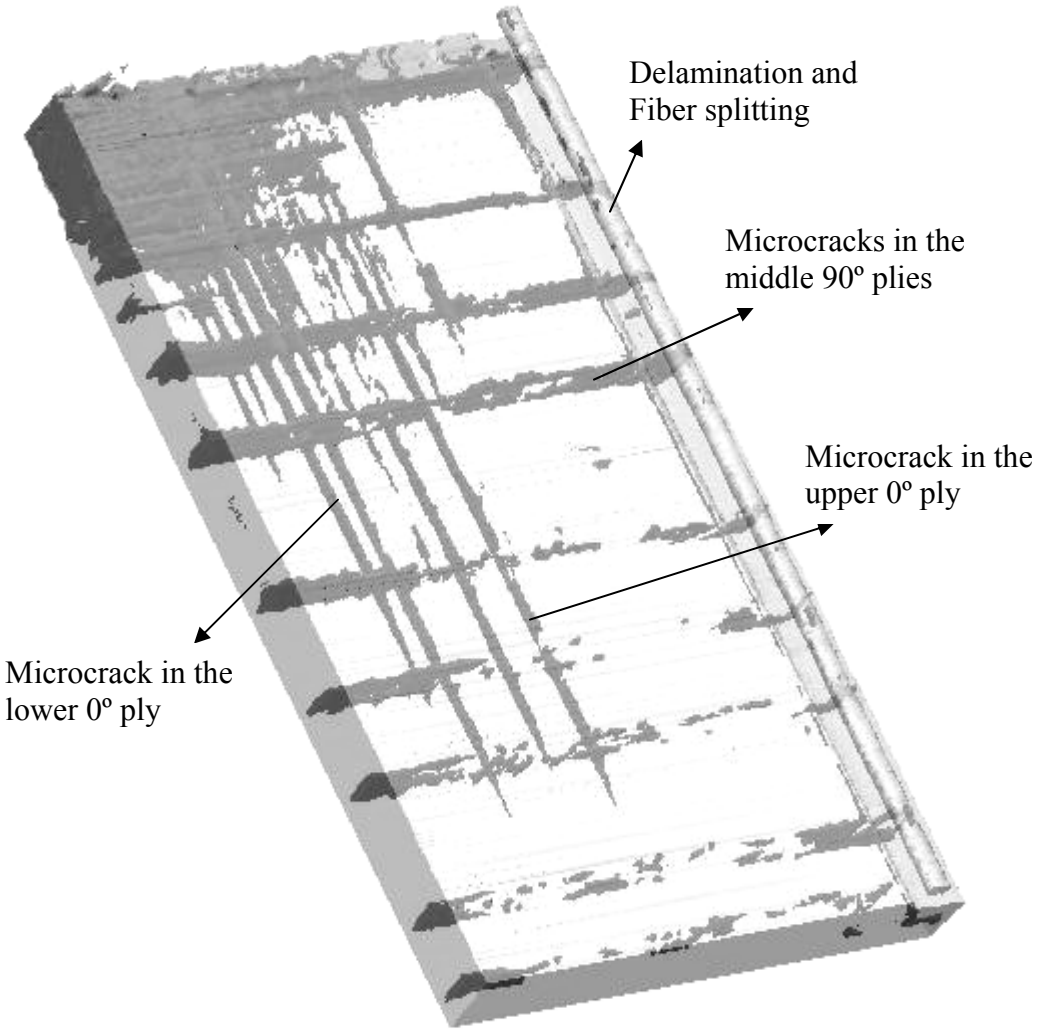

Figure 5.10 *Three Dimensional Model of Sample from IM7/5276-1 loaded to 1060MPa*

In Figure 5.11 we can see a similar 3D model of sample from the same IM7/5276-1 material system loaded to 1100MPa. In this sample it was observed that a higher number of microcracks formed in the middle 90º plies and the material failed following microcracks in the 0º plies along with delamination and fiber splitting. In the model we can see a portion of approximately 4mm x 3mm of the sample. The microcracks in the

90º plies of this sample correspond to crack density of 14.5 cm^{-1} in Figure 5.3. At this stress level, the sample failed completely following delamination and fiber splitting. Due to extensive failure only a small portion of the sample was modeled three dimensionally as shown.

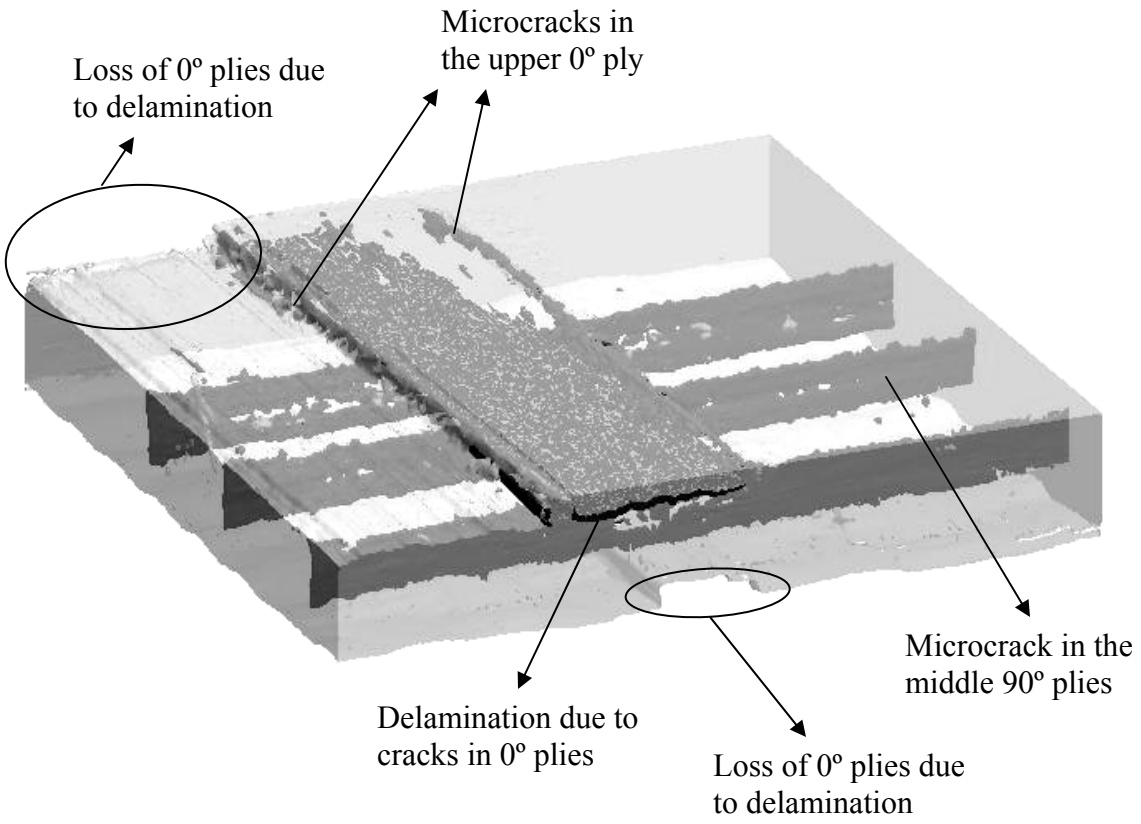

Figure 5.11 *Three Dimensional Model of Sample from IM7/5276-1 loaded to 1100MPa*

In the 3D model above, microcracks in the 90º and 0º can be observed along with extensive damage caused due to delamination. We can observe that there is loss of sections of the outer 0º plies caused due to delamination. A strip along the left edge of the top 0º ply and a strip along the middle of the bottom 0º ply are missing due to

delamination. A strip along the middle of the top 0º ply is still intact with the material showing the delamination caused due to microcracks in the top 0º ply. The dark region below the delaminated ply is due to pooling of the dye. A top view of the same sample is shown in the Figure 5.12 where the loss of section in the outer 0º plies can be seen clearly.

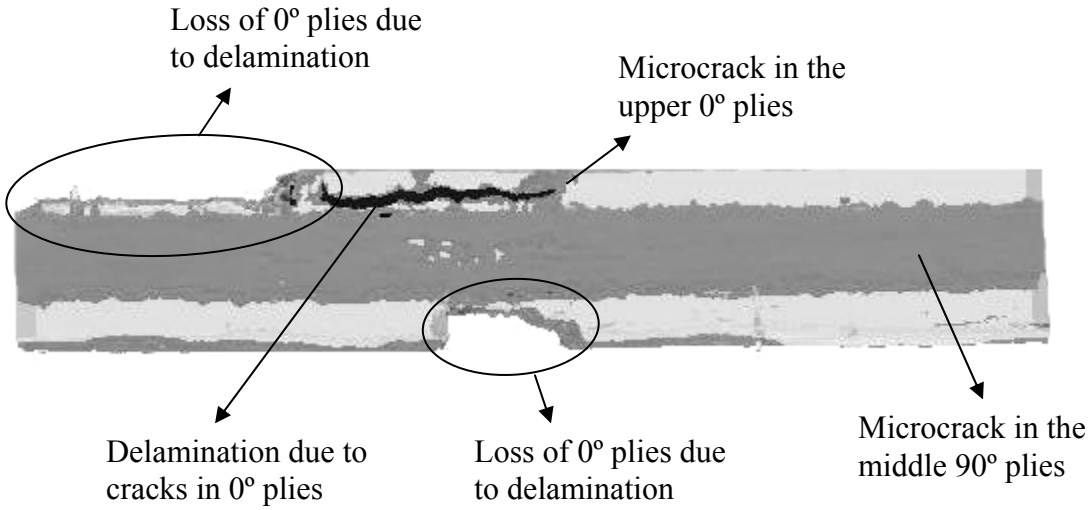

Figure 5.12 *Three Dimensional Model of Sample from IM7/5276-1 loaded to 1100MPa*

6. Conclusions

All the three material systems IM7/977-2, IM7/5555 and IM7/5276-1 with $[0/90]_s$ orientation are resistant to microcracking below 800MPa of stress in Mode I loading. As the stress reaches above 800MPa onset of microcracking is observed in the IM7/5555 material at 850MPa, in the IM7/5276-1 material at 900MPa and in the IM7/977-2 material at 1100MPa. IM7/977-2 is most resistant to microcracking and IM7/5555 is the least resistant to microcracking. A significant observed phenomenon by looking at the failure stresses was that the IM7/5276-1 material system has the weakest failure stress around 1100MPa, which is the stress required to initiate microcracking in IM7/977-2 material. Looking at the crack density saturation for the above three materials, IM7/977-2 has a slightly lower crack density saturation compared to others. Several samples failed before reaching their expected failure stresses; this might be because of the inaccuracy to maintain constant cross-sectional area of the sample and improper adhesion of the tabs.

It is observed that one of the samples from the IM7/5555 material system contained voids and delamination in it. It was observed that the sample which had these defects showed low crack density even at higher stress level, compared to other samples of the same system. This indicates that the statistical inhomogeneities or manufacturing defects probably broadened the sloped portion of the crack density curve for this sample. This can be supported from Nairn's research paper on microcracking Ref [27]. The IM7/5555

samples showed more scatter in data points compared to the other two material systems which may be because of the inhomogeneity in the material. A popping noise was observed during loading of the specimen which may be the indication for fiber breakage.

X-ray microtomography provides an excellent tool for characterizing the microcracks and damage connectivity in composites at different stress levels. The 3D models shown in chapter 3, created by using this technique, provide excellent information about the damage geometry and connectivity. For example excellent information was obtained about the connectivity of the damage due to microcracks in the 90º and 0º plies and the delamination connecting the microcracks. This damage connectivity would act as an excellent path of leakage in cryogenic application. Further study of data at loads near failure is recommended to get more information about damage connectivity.

From the above experimental work, out of the three material systems, IM7/977-2 is the most resistant to microcracking. Further studies are required to find more information on microcracking at cryogenic temperatures which is another aspect of thermo-mechanical loading. With the above knowledge of uni-axial testing, it is recommended that bi-axial loads be applied to the materials to learn more about microcracks and damage connectivity.

REFERENCES

1. Dixon. S.C, Tenny. D.R, Rummler. D.R, Weiting. A and Bader. M, *"Structures and Material Technology Issues for Reusable Launch Vehicles,"* NASA TM-87626, October 1985.
2. Kessler S.S, *"Cryocycling and Mechanical Testing of CFRP for the X-33 LH2 Fuel Tank Structure."* Massachusetts Institute of Technology, S.B., TELAC Report # 98-15, May 1998.
3. *"Final Report of the X-33 Failure Investigation Team,"* X-33: Reusable Launch Vehicle – Space Transportation [online database], URL: http://x33.msfc.nasa.gov [cited 24 Jan. 2001]
4. Simon Frost, Richard Lee, Mark Stone, *"Assessment & Criticality of Defects & Damage in Materials Systems"* Task 1 Review, AEA Technology, MMS13 IAG, November 2002.
5. Michael Gower, Graham Sims*, "Assessment & Criticality of Defects & Damage in Materials Systems"* Task 1 Review, National Physical Laboratory, MMS13 IAG, November 2002.
6. R. Joffe*, "Damage Accumulation and Stiffness Degradation in Composite Laminates",* Doctoral Thesis.
7. Kunigal N. Shiva Kumar, *"Course MEEN860 – Fracture Mechanics"*, North Carolina A&T State University.
8. J. A. Nairn and S. Hu, *"Micromechanics of Damage: A Case Study of Matrix Microcracking"*. In Damage Mechanics of Composite Materials, ed., Ramesh Talreja, Elsevier, Amsterdam (1994), pp.187-243.
9. R. P. Crossman and M. G. Bader, *"Damage Development in CRPF Laminates under Monotonic and Cyclic stressing"*, Fiber Science Technology, Volume-18 (1983), pp.163-180.
10. D. L. Flaggs and M. H. Kural, *"Experimental Determination of the In-Situ Transverse Lamina Strength in Graphite Epoxy Laminate"*, Journal of Composite Materials, Volume-16 (1982), pp.103-116.

11. S. E. Groves, C. E. Harris, A. L. Highsmith, and R. G. Norvell, *"An Experimental and Analytical Treatment of Matrix Cracking in Cross-Ply Laminates"*, Experimental Mechanics, March (1987), pp. 73-79.
12. S. Hu, J. S. Bark, and J. A. Nairn, *"On the Phenomenon of Curved Microcracks in [0m/90n]s Laminates: Their Shapes, Initiation Angles, and Locations"*, Composite Science. & Technology, Volume- 47 (1993), pp. 321-329.
13. K. W. Garrett and J. E. Bailey, *"Multiple Transverse Fracture in 90± Cross-Ply Laminates of a Glass Fiber-Reinforced Polyester"*. Journal of Material Science, Volume-12 (1977), pp.157-168.
14. K. W. Garrett and J. E. Bailey, *"The Effect of Resin Failure Strain on the Tensile Properties of Glass Fiber-Reinforced Cross-Ply Laminates"*. Journal of Material Science, Volume-12 (1977), pp.2189-2194.
15. A. Parvizi, K. W. Garrett, and J. E. Bailey, *"Constrained Cracking in Glass Fiber-Reinforced Epoxy Cross-Ply Laminates"*. Journal of Material Science, Volume-13 (1978), pp.195-201.
16. M. G. Bader, J. E. Bailey, P. T. Curtis, and A. Parvizi, *"The Mechanisms of Initiation and Development of Damage in Multi-Axial Fiber-Reinforced Plastics Laminates"*. Proceedings of 3rd Int'l Conf. on Mechanical Behavior of Materials 3 (1979), pp.227-239.
17. J. E. Bailey, P. T. Curtis and A. Parvizi, *"On the Transverse Cracking and Longitudinal Splitting Behavior of Glass and Carbon Fiber Epoxy Cross-Ply Laminates and the Effect of Poisson and Thermally Generated Strains"*. Proc. R. Soc. Lond. A 366 (1979), pp.599-623.
18. D. L. Flaggs and M. H. Kural, *"Experimental Determination of the In Situ Transverse Lamina Strength in Graphite/Epoxy Laminates"*. Journal of Material Science, Volume-16 (1982), pp.103-115.
19. W. W. Stinchcomb, K. L. Reifsnider, P. Yeung, and J. Masters, *"Effect of Ply Constraint on Fatigue Damage Development in Composite Material Laminates"*. ASTM STP 723 (1981), pp.64-84.
20. A. L. Highsmith and K. L. Reifsnider, *"Stiffness-Reduction Mechanisms in Composite Laminates"*. ASTM STP 775 (1982), pp.103-117.

21. J. A. Nairn, S. Hu, S. Liu, and J. S. Bark, *"The Initiation, Propagation, and Effect of Matrix Microcracks in Cross-Ply and Related Laminates"*. Proc. of the 1st NASA Advanced Composite Tech. Conf. Seattle, WA, Oct. 29 to Nov. 1, 1990 (1990).
22. J. A. Nairn, *"Microcracking, Microcrack-Induced Delamination, and Longitudinal Splitting of Advanced Composite Structures"*. NASA CR 4472 (1992).
23. J. A. Nairn and S. Hu, *"The Formation and Effect of Outer-Ply Microcracks in Cross-Ply Laminates: A Variational Approach"*. Engineering Fracture Mechanics, Volume-41 (1992), pp.203-221.
24. L. Berglund and J. Varna, *"Transverse Cracking and Local Delamination in [04=90n]s and [90n=04]s Carbon Fiber/Toughened Epoxy Laminates"*. Journal of Reinforced Plastic & Composites. Volume-11 (1992), pp.643-660.
25. P. A. Smith, L. Boniface, and N. F. C. Glass, *"A Comparison of Transverse Cracking Phenomena in (0/90)s and (90/0)s CFRP Laminates"*. Applied Composite Materials. Volume-5 (1998), pp.11-23.
26. J. A. Lavoie, E. Adolfsson, *"Stitch Cracks in Constraint Plies Adjacent to a Cracked Ply"*, Journal of Composite Materials, Volume-35, Number-23 (2001), pp. 2077-2097.
27. J. A. Nairn, *"Matrix Microcracking in Composites"*. Polymer Matrix Composites (edited by R. Talreja and J.-A. E. Manson), Volume-2 of Comprehensive Composite Materials, Elsevier Science, pp.403-432 (2000).
28. Brewer J C and Lagace P A, *"Quadratic stress criterion for initiation of delamination"*, Journal of composite materials, Volume-22 (1988), pp.1141-1155.
29. Zhang J, Soutis C and Fan J, *"Strain energy release rate associated with local delamination in cracked composite laminates"*, Composites, Volume-25 (1984), pp 851-862.
30. Nairn J A and Hu S, *"The initiation and growth of delaminations induced by matrix microcracks in laminated composites"*, International Journal of Fracture, Volume-57 (1992), pp 1-24.

31. M. A. Stone, *"MMS Project 13 Assessment and criticality of damage and defects in material systems"*, Task 5 Report - Review and identification of methods for analysing the effects of defects and damage, AEA Technology, March 2003.
32. Mandell J F, Samborsky D D, Scott M E and Cairns D S, *"Effects of structural details on delamination and fatigue life of fiberglass laminates"*, AIAA Paper 98-0061, AIAA, 1998.
33. Conti P and De Paulis A, 'A simple method to simulate the interlaminar stresses generated near the free edge of a composite laminate', *Delamination and debonding of materials,* ASTM STP 876, ASTM, 1985, pp 35-51.
34. O'Brien K T, *"Analysis of local delaminations and their influence on composite laminate behavior"*, Delamination and debonding of materials*,* ASTM STP 876, American Society for Testing and Materials, 1985, pp 282-297.
35. K. L. Reifsnider, W. W. Stinchcomb, E. G. Henneke and J. C. Duke, *"Fatigue Damage Strength Relationships in Composite Laminates"*, AFWALTR-83-3804, Air Force Wright Aeronautical Laboratories, Ohio, 1983.
36. R. D. Jamison and K. L. Reifsnider, *"Advanced Fatigue Damage Development in Graphite Epoxy laminates"*, AFWAL-TR-82-3103, Air Force Wright Aeronautical Laboratories, Ohio, 1982.
37. J. T. Ryder and F. W. Crossman, *"A Study of Stiffness, Residual Strength and Fatigue Life Relationships for Composite Laminates"*, NASA-CR-172211, Lanley Research Centre, Hampton, Virginia, 1983.
38. A. S. D. Wang, N. N. Kishore, C. A. Li, *"Crack Development in Graphite Epoxy Cross-Ply Laminates under Uniaxial Loading"*, Composite Science & Technology, Volume-24 (1985), pp.1-31.
39. Los Alamos National Laboratory, Engineering Sciences & Applications (ESA) Division. URL – "*http://www.nde.lanl.gov/default.htm".*
40. W. C. Rontgen, Analytical Physics and Chemistry, 1898, Volume-64, (1), pp.1-37.
41. J. A. Rowlands, *"Current Advances and Future Trends in X-Ray Digital Detectors for Medical Applications,"* IEEE Trans. Instr. and Meas., Volume-47, pp.1415-1418 (1998)

42. J. A. Rowlands, *"The Physics of Computed Radiography",* Phys. Med. Biol., Voluem-47 (2002), pp.R123-R166.

43. Bray D. E. and Stanley R. K., *"Non Destructive Evaluation: a tool in design, manufacturing, and service"*. CRC Press, Inc., FL, 1997.

44. G. P. Yost, PhD, *"Intrinsity™ FastMATH™ Application to Computed Tomography",* Version 1.2, URL - *"http://www.intrinsity.com"*

45. NDT Resource Centre, at URL – *http://www.ndt-ed.org*

46. Crane, R. L., *"A New Penetrant for Composites and Adhesively Bonded Structures",* Materials Evaluation, Volume 35, No. 2, Feb. 1877, pp. 54-55

47. BhanuPrakash Karedla *"Detection of Damage in Fiber Reinforced Composites by X-Ray Microtomography"*, A Thesis report – University of New Orleans, May 2003.

Vita

Arun Kumar Tatiparthi was born on January 3, 1978 to Ramamurthy and Venkatalakshmi Tatiparthi in Kakinada, India. He was raised in Visakhapatnam a coastal city of India and graduated from Dr. L. B. Junior College in 1995 and obtained his Bachelor of Technology degree in Mechanical Engineering from Nagarjuna University in 2000. He then continued on with graduate school at University of New Orleans and accepted a position as a graduate research assistant working for Dr. Paul J. Schilling on the NCAM project in the August of 2001. In May of 2004, he earned his Masters of Science degree in Mechanical Engineering with a thesis entitled "Investigation Of Microcrack Growth In $[0/90]_S$ Graphite Epoxy Composite Laminates Using X-Ray Microtomography."